

## Meson-exchange model for $\pi N$ scattering and $\gamma N \rightarrow \pi N$ reaction

T. Sato<sup>1,2</sup> and T.-S. H. Lee<sup>1</sup>

<sup>1</sup>Physics Division, Argonne National Laboratory, Argonne, Illinois 60439-4843

<sup>2</sup>Department of Physics, Osaka University, Toyonaka, Osaka 560, Japan

(Received 7 June 1996)

An effective Hamiltonian consisting of bare  $\Delta \leftrightarrow \pi N$ ,  $\gamma N$  vertex interactions and energy-independent meson-exchange  $\pi N \leftrightarrow \pi N$ ,  $\gamma N$  transition operators is derived by applying a unitary transformation to a model Lagrangian with  $N, \Delta, \pi, \rho, \omega$ , and  $\gamma$  fields. With appropriate phenomenological form factors and coupling constants for  $\rho$  and  $\Delta$ , the model can give a good description of  $\pi N$  scattering phase shifts up to the  $\Delta$  excitation energy region. It is shown that the best reproduction of the recent LEGS data of the photon-asymmetry ratios in  $\gamma p \rightarrow \pi^0 p$  reactions provides rather restricted constraints on the coupling strengths  $G_E$  of the electric  $E2$  and  $G_M$  of the magnetic  $M1$  transitions of the bare  $\Delta \leftrightarrow \gamma N$  vertex and the less well-determined coupling constant  $g_{\omega NN}$  of  $\omega$  meson. Within the ranges that  $G_M = 1.9 \pm 0.05$ ,  $G_E = 0.0 \pm 0.025$ , and  $7 \leq g_{\omega NN} \leq 10.5$ , the predicted differential cross sections and photon-asymmetry ratios are in an overall good agreement with the data of  $\gamma p \rightarrow \pi^0 p$ ,  $\gamma p \rightarrow \pi^+ n$ , and  $\gamma n \rightarrow \pi^- p$  reactions from 180 MeV to the  $\Delta$  excitation region. The predicted  $M_{1+}$  and  $E_{1+}$  multipole amplitudes are also in good agreement with the empirical values determined by the amplitude analyses. The constructed effective Hamiltonian is free of the nucleon renormalization problem and hence is suitable for nuclear many-body calculations. We have also shown that the assumptions made in the  $K$ -matrix method, commonly used in extracting empirically the  $\gamma N \rightarrow \Delta$  transition amplitudes from the data, are consistent with our meson-exchange dynamical model. It is found that the helicity amplitudes calculated from our bare  $\gamma N \rightarrow \Delta$  vertex are in good agreement with the predictions of the constituent quark model. The differences between these bare amplitudes and the dressed amplitudes, which are closer to the empirical values listed by the Particle Data Group, are shown to be due to the nonresonant meson exchange mechanisms. Within the range  $7 \leq g_{\omega NN} \leq 10.5$  of the  $\omega$  meson coupling favored by the data of the photon-asymmetry ratios in  $\gamma p \rightarrow \pi^0 p$  reactions, our values of the  $E2/M1$  ratio for the  $\gamma N \rightarrow \Delta$  transition are  $(0.0 \pm 1.3)\%$  for the bare vertex and  $(-1.8 \pm 0.9)\%$  for the dressed vertex. [S0556-2813(96)04611-0]

PACS number(s): 13.75.Gx, 21.45.+v, 24.10.-i, 25.20.Lj

### I. INTRODUCTION

The main objective of investigating photoproduction and electroproduction of mesons on the nucleon is to study the structure of the nucleon excited states ( $N^*$ ). This has been pursued actively [1] during the period around 1970. With the developments at several electron facilities since 1980, more extensive investigations of the  $\Delta$  excitation have been carried out both experimentally and theoretically [2]. Apart from the need for precise and extensive measurements which will soon be possible at CEBAF and Mainz, an accurate understanding of the  $N^*$  structure can be obtained only when an appropriate reaction theory is developed to separate the reaction mechanisms from the hadron structure in the  $\gamma N \rightarrow \pi N$ ,  $\pi \pi N$  reactions. The importance of this theoretical effort can be understood by recalling many years experiences in the development of nuclear physics. For example, the information about the deformation of  $^{12}\text{C}$  can be extracted from  $^{12}\text{C}(p, p')^{12}\text{C}^*(2^+, 4.44 \text{ MeV})$  inelastic scattering only when a reliable reaction theory [3], such as the distorted-wave impulse approximation or the coupled-channels method, is used to calculate the initial and final proton- $^{12}\text{C}$  interactions. Accordingly, one expects that the  $N^*$  structure can be determined only when the interactions in its decay channels  $\gamma N$ ,  $\pi N$ , and  $\pi \pi N$  can be calculated from a reliable reaction theory. It is the objective of this work to address this problem from the point of view of meson exchange models. In contrast to approaches based on the dispersion

relations [1] or the  $K$ -matrix method [4–7], our approach is aimed at not only an investigation of the  $N^*$  structure but also at the application of the constructed model to a consistent calculation of  $N^*$  in nuclear many-body systems.

The meson-exchange models have been very successful in describing nucleon-nucleon interactions [8], electroweak interaction currents [9,10], meson-meson scattering [11], and meson-nucleon scattering [12–14]. It is therefore reasonable to expect that the same success can also be achieved in the investigation of pion photoproduction and electroproduction. This possibility has, however, not been fully explored. The dynamical models of pion photoproduction developed in Refs. [15–17] did contain the well-established meson exchange mechanisms of pion photoproduction, but phenomenological separable potentials were used to describe the  $\pi N$  multiple scattering. The improvement made in Ref. [18] suffered from the theoretical inconsistency in defining the meson exchange  $\pi N$  interaction and  $\pi N \rightarrow \gamma N$  transition. The model developed in Refs. [19,20] also does not treat meson exchange completely since a zero-range contact term is introduced to replace the particle-exchange terms of their  $\pi N$  potential. In all of these models, the incomplete treatment of the meson-exchange interactions leads to some uncertainties in interpreting the parameters characterizing the  $\gamma N \rightarrow \Delta$  vertex which is the main interest in testing hadron models. The formulation developed in Ref. [21] can, in principle, be used to examine the meson-exchange mechanisms in pion photoproduction, but has not been pursued numeri-

cally. In this work, we will try to improve the situation by applying the unitary transformation method developed in Ref. [22] to derive from a model Lagrangian an effective Hamiltonian for a consistent meson-exchange description of both the  $\pi N$  scattering and pion photoproduction. Furthermore, the constructed model can be directly used to improve and extend the  $\pi NN$  Hamiltonian developed in Ref. [23] to also describe the electromagnetic  $\Delta$  excitation in intermediate energy nuclear reactions.

The starting point of constructing a meson-exchange model is a model Lagrangian of relativistic quantum field theory. The form of the Lagrangian is constrained by the observed symmetries of fundamental interactions, such as Lorentz invariance, isospin conservation, chiral symmetry, and gauge invariance. The most common approach [24] is to find an appropriate three-dimensional reduction of the ladder Bethe-Salpeter equation of the considered model Lagrangian. The meson-exchange potentials are then identified with the driving terms of the resulting three-dimensional scattering equation. The most recent examples are the  $\pi N$  models developed in Refs. [12–14,19]. The extension of this approach to investigate pion photoproduction has also been made in Ref. [20].

Alternatively, one can construct a meson-exchange model by deriving an effective Hamiltonian from the considered model Lagrangian. Historically, two approaches have been developed. The first one is to use the Tamm-Dancoff approximation [25]. This method leads to an effective Hamiltonian which is energy dependent and contains unlinked terms, and hence cannot be easily used in nuclear many-body calculations. A more tractable approach is to apply the method of unitary transformation which was developed by Fukuda, Sawada, and Taketani [26] and independently by Okubo [27]. This approach, called the FST-Okubo method, has been very useful in investigating nuclear electromagnetic currents [28–30] and relativistic descriptions of nuclear interactions [31–34]. The advantage of this approach is that the resulting effective Hamiltonian is energy independent and can readily be used in nuclear many-body calculation. Motivated by the investigation of the  $\pi NN$  dynamics [23,35], this method has been extended in Ref. [22] to derive an effective theory involving pion production channels. In this work, we adopt this method to develop a dynamical model for  $\pi N$  scattering and  $\gamma N \rightarrow \pi N$  reactions.

It is necessary to explain here how our approach is related to the approach based on chiral perturbation theory (CHPT) [36]. Since chiral symmetry is a well-established dynamical symmetry of strong interactions, it should be used to constrain our starting Lagrangian. This leads us to assume that our starting Lagrangian is an effective Lagrangian for generating the tree diagrams in CHPT. The parameters are then completely determined by the well-established chiral dynamics such as partially conserved axial-vector current (PCAC) and current algebra. Therefore, our model and CHPT are identical in leading orders. The differences come from how the unitarity is implemented to account for the  $\pi N$  multiple scattering. In the spirit of CHPT, the ‘low’-momentum pions are considered as weakly interacting Goldstone bosons and hence their interactions with the nucleon can be treated as perturbations [37]. This amounts to restoring the unitarity perturbatively by calculating loop corrections order by order.

It is then necessary to include more terms in the effective Lagrangian. A phenomenological procedure is then unavoidable to determine the accompanied low-energy constants.

In the meson-exchange model, one hopes to describe the  $\pi N$  multiple scattering in the entire kinematic region including the highly nonperturbative  $\Delta$  excitation region. The essential assumption is that the  $\pi N$  multiple scattering is governed by a few-body Schrödinger equation with the driving terms calculated from the starting Lagrangian in a perturbation expansion in the coupling constants. This can be realized in practice only when the driving terms are regularized by appropriate phenomenological form factors. Qualitatively speaking, the meson-exchange model is an alternative to CHPT in the kinematic region where perturbative calculations become very difficult or impossible. Both approaches involve phenomenological parameters. The success of each approach depends on whether these parameters can be interpreted theoretically.

In this work we will focus on the  $\Delta$  excitation and will limit our investigation to the energy region where  $2\pi$  production is negligibly small. By applying the unitary transformation of Ref. [22] to a model Lagrangian for  $N$ ,  $\Delta$ ,  $\pi$ ,  $\rho$ ,  $\omega$ , and  $\gamma$  fields, we have obtained an effective Hamiltonian consisting of bare  $\Delta \leftrightarrow \pi N$ ,  $\gamma N$  vertex interactions and energy-independent  $\pi N \leftrightarrow \pi N$ ,  $\gamma N$  transition operators. The  $\pi N$  scattering phase shifts [38–40] are used to determine the hadronic part of the constructed effective Hamiltonian which has only seven parameters for defining the vertices of the meson-exchange  $\pi N$  potential and the  $\Delta \leftrightarrow \pi N$  transition. The strong vertex functions in the  $\gamma N \rightarrow \pi N$  transition operator are then also fixed. This is a significant improvement over the previous dynamical models [15–17] in which the employed separable potentials have no dynamical relation with the pion photoproduction operator. A consistent description of the  $\pi N$  scattering and  $\gamma N \rightarrow \pi N$  transition is crucial for separating the reaction mechanisms due to meson-exchange nonresonant interactions from the total  $\gamma N \rightarrow \Delta$  transition.

Once the hadronic part of the effective Hamiltonian is determined, the resulting pion photoproduction amplitude has only three adjustable parameters:  $G_M$  of magnetic  $M1$  and  $G_E$  of electric  $E2$  transitions of the bare  $\gamma N \rightarrow \Delta$  vertex, and the less well-determined  $\omega NN$  coupling constant. We will determine these three parameters by considering the most recent LEGS data [41] of the photon-asymmetry ratios in  $\gamma p \rightarrow \pi^0 p$  reactions. The resulting parameters are then tested against very extensive data in Refs. [42–44].

It is customary to test hadron models by comparing the theoretical predictions of  $N^* \rightarrow \gamma N$  transition amplitudes with the empirical values listed by the Particle Data Group (PDG) [45]. Since the first systematic calculation [46] based on the constituent quark model was performed, it has been observed that the predicted  $\Delta \rightarrow \gamma N$  transition amplitudes [46–50] are significantly smaller than the empirical values listed by the PDG [45]. While the problem may be due to the limitations of the constituent quark model, it is necessary to recognize that the empirical values of the PDG are obtained by using the  $K$ -matrix method [4–7] or dispersion relation [1]. Both approaches contain assumptions about the nonresonant contributions to the  $\gamma N \rightarrow \Delta$  transition and must be justified from a dynamical point of view. Within our dynamical

model, we will address this point concerning the  $K$ -matrix method. This leads us to identify our bare  $\gamma N \rightarrow \Delta$  vertex with the constituent quark model. The dispersion relation approach [1,51] is defined in a very different theoretical framework and therefore is beyond the scope of this investigation.

In Sec. II, we will use a simple model Lagrangian to explain how an effective Hamiltonian can be constructed by using the unitary transformation method of Ref. [22]. The method is then applied to realistic Lagrangians to derive in Secs. III and IV an effective Hamiltonian for  $\pi N$  scattering and pion photoproduction. The equations for calculating the  $\pi N$  scattering and  $\gamma N \rightarrow \pi N$  amplitudes are also presented there. The relationships with the  $K$ -matrix method are then established. Results and discussions are given in Sec. V. The conclusions and discussions of future studies are given in Sec. VI.

## II. METHOD OF UNITARY TRANSFORMATION

To explain the unitary transformation method of Ref. [22] [will be referred to as the Sato-Kobayashi-Ohtsubo (SKO)

method], it is sufficient to consider a simple system consisting of only neutral pions and fictitious  $\sigma$  mesons. The objective is to derive an effective Hamiltonian from the Lagrangian density

$$L(x) = L_0(x) + L_I(x), \quad (2.1)$$

where  $L_0(x)$  is the usual noninteracting Lagrangian, and the interaction term is taken to be

$$L_I(x) = -g_{\sigma\pi\pi} \phi_\pi^2(x) \phi_\sigma(x). \quad (2.2)$$

The Hamiltonian can be derived from Eq. (2.1) by using the standard method of canonical quantization. In the second-quantization form, we obtain (in the convention of Bjorkin and Drell [52])

$$H = H_0 + H_I, \quad (2.3)$$

with

$$H_0 = \int d\vec{k} [E_\pi(k) a^\dagger(\vec{k}) a(\vec{k}) + E_\sigma(k) b^\dagger(\vec{k}) b(\vec{k})], \quad (2.4)$$

$$H_I = g_{\sigma\pi\pi} \int \frac{d\vec{k}_1 d\vec{k}_2 d\vec{k}}{\sqrt{(2\pi)^3 8 E_\pi(k_1) E_\pi(k_2) E_\sigma(k)}} \{ [2a^\dagger(\vec{k}_1) a(\vec{k}_2) b(\vec{k}) \delta(\vec{k}_1 - \vec{k}_2 - \vec{k}) + a^\dagger(\vec{k}_1) a^\dagger(\vec{k}_2) b(\vec{k}) \delta(\vec{k}_1 + \vec{k}_2 - \vec{k}) + a(\vec{k}_1) a(\vec{k}_2) b(\vec{k}) \delta(\vec{k}_1 + \vec{k}_2 + \vec{k})] + [\text{H.c.}] \}, \quad (2.5)$$

where  $a^\dagger(\vec{k})$  and  $b^\dagger(\vec{k})$  are, respectively, the creation operators for  $\pi$  and  $\sigma$  particles,  $E_\alpha(k) = \sqrt{m_\alpha^2 + k^2}$  is the free energy for the particle  $\alpha$ , and [H.c.] means taking the Hermitian conjugate of the first term in the equation. We further assume that the mass of the  $\sigma$  meson is heavier than two-pion mass, i.e.,  $m_\sigma > 2m_\pi$ .

Because of the intrinsic many-body problem associated with the starting quantum field theory, it is not possible to solve exactly the equation of motion for meson-meson scattering defined by the above Hamiltonian. A simplification is obtained by assuming that in the low- and intermediate-energy regions, only ‘‘few-body’’ states are active and must be treated explicitly. The effects due to ‘‘many-body’’ states are absorbed in effective interaction operators which can be calculated in a perturbation expansion in coupling constants. This few-body approach to field theory was pioneered by Amado and Aaron [53]. In the SKO approach, this is achieved by first decomposing the interaction Hamiltonian  $H_I$ , Eq. (2.5), into two parts:

$$H_I = H_I^P + H_I^Q \quad (2.6)$$

$$H_I^P = g_{\sigma\pi\pi} \int \frac{d\vec{k}_1 d\vec{k}_2 d\vec{k}}{\sqrt{(2\pi)^3 8 E_\pi(k_1) E_\pi(k_2) E_\sigma(k)}} \times \{ a^\dagger(\vec{k}_1) a^\dagger(\vec{k}_2) b(\vec{k}) \delta(\vec{k}_1 + \vec{k}_2 - \vec{k}) + [\text{H.c.}] \}, \quad (2.7)$$

$$H_I^Q = g_{\sigma\pi\pi} \int \frac{d\vec{k}_1 d\vec{k}_2 d\vec{k}}{\sqrt{(2\pi)^3 8 E_\pi(k_1) E_\pi(k_2) E_\sigma(k)}} \times \{ [2a^\dagger(\vec{k}_1) a(\vec{k}_2) b(\vec{k}) \delta(\vec{k}_1 - \vec{k}_2 - \vec{k}) + a(\vec{k}_1) a(\vec{k}_2) b(\vec{k}) \delta(\vec{k}_1 + \vec{k}_2 + \vec{k})] + [\text{H.c.}] \}. \quad (2.8)$$

The elementary processes induced by  $H_I^P$  are illustrated in the upper half of Fig. 1. For  $m_\sigma > 2m_\pi$ , the  $\sigma \rightarrow \pi\pi$  decay and  $\pi\pi \rightarrow \sigma$  annihilation are ‘‘real processes’’ and can take place in free space. On the other hand, the processes  $\pi \leftrightarrow \pi\sigma$  and vacuum  $\leftrightarrow \pi\pi\sigma$  induced by  $H_I^Q$  are ‘‘virtual processes’’ (lower part of Fig. 1). They cannot occur in free space because of the energy-momentum conservation. The

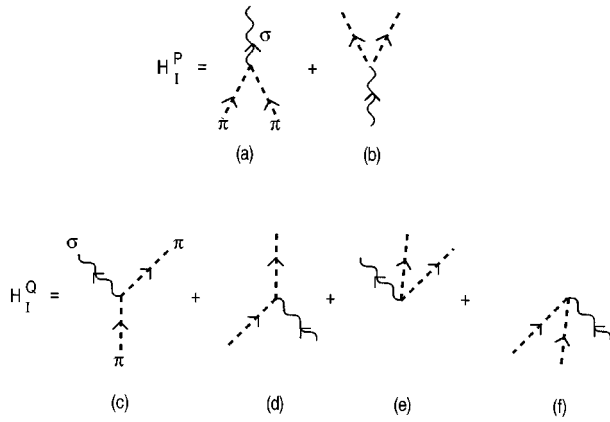


FIG. 1. Graphical representation of the interaction Hamiltonians  $H_I^P$  of Eq. (2.7) and  $H_I^Q$  of Eq. (2.8).

essence of the SKO method is to systematically eliminate the virtual processes from the considered Hamiltonian by using unitary transformations. As a result the effects of "virtual processes" are included as effective operators in the transformed Hamiltonian.

The transformed Hamiltonian is defined as

$$\begin{aligned} H' &= UH U^\dagger \\ &= U(H_0 + H_I^P + H_I^Q)U^\dagger, \end{aligned} \quad (2.9)$$

where  $U = \exp(-iS)$  is a unitary operator defined by a Hermitian operator  $S$ . By expanding  $U = 1 - iS + \dots$ , the transformed Hamiltonian can be written as

$$\begin{aligned} H' &= H_0 + H_I^P + H_I^Q + [H_0, iS] + [H_I, iS] \\ &+ \frac{1}{2!} [[H_0, iS], iS] + \dots \end{aligned} \quad (2.10)$$

To eliminate from Eq. (2.10) the virtual processes which are of first order in the coupling constant  $g_{\sigma\pi\pi}$ , the SKO method imposes the condition that

$$H_I^Q + [H_0, iS] = 0. \quad (2.11)$$

Since  $H_0$  is a diagonal operator in Fock space, Eq. (2.11) clearly implies that  $iS$  must have the same operator structure of  $H_I^Q$ .

To simplify the presentation, we write  $H^Q$  as

$$H_I^Q = \sum_n \int F_n O_n d\vec{k}_1 d\vec{k}_2 d\vec{k}, \quad (2.12)$$

where  $O_n$  denotes the part containing the creation and annihilation operators, and  $F_n$  is the rest of the  $n$ th term in Eq. (2.8). In the form of Eq. (2.12), the solution of Eq. (2.11) can be written as

$$iS = \sum_n i \int S_n O_n d\vec{k}_1 d\vec{k}_2 d\vec{k}. \quad (2.13)$$

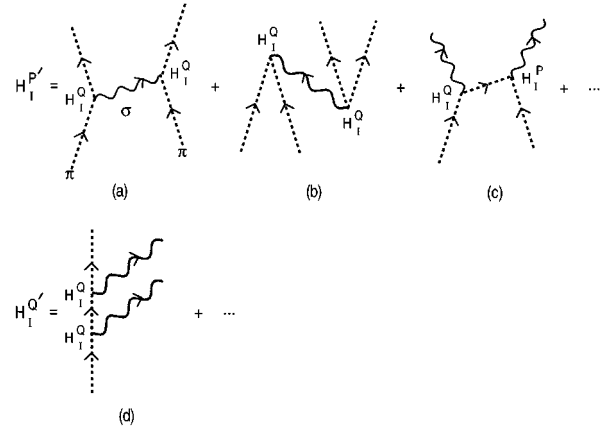


FIG. 2. Graphical representation of the effective interaction Hamiltonians  $H_I^{P'}$  of Eq. (2.19) and  $H_I^{Q'}$  of Eq. (2.20).

Our task is to find  $S_n$  by solving Eq. (2.11). Considering two eigenstates  $|i\rangle$  and  $|f\rangle$  of the free Hamiltonian  $H_0$  such that  $\langle f|O_n|i\rangle = 1$ , Eqs. (2.11), (2.12), and (2.13) then lead to

$$iS_n = \frac{-1}{E_f - E_i} F_n. \quad (2.14)$$

Note that  $E_i$  and  $E_f$  are the eigenvalues of free Hamiltonian  $H_0$ , and hence the solution  $S_n$  is independent of the collision energy  $E$  of the total Hamiltonian  $H$ . This is an important feature distinguishing our approach from the Tamm-Dancoff approximation. By using the above relation, it is easy to verify that the solution of the operator equation (2.11) is

$$\begin{aligned} iS &= g_{\sigma\pi\pi} \int \frac{d\vec{k}_1 d\vec{k}_2 d\vec{k}}{\sqrt{(2\pi)^3 8 E_\pi(k_1) E_\pi(k_2) E_\sigma(k)}} \\ &\times \left( \left[ 2a^\dagger(\vec{k}_1) a(\vec{k}_2) b(\vec{k}) \frac{\delta(\vec{k}_1 - \vec{k}_2 - \vec{k})}{-E_\pi(k_1) + E_\pi(k_2) + E_\sigma(k)} \right. \right. \\ &\left. \left. + a(\vec{k}_1) a(\vec{k}_2) b(\vec{k}) \frac{\delta(\vec{k}_1 + \vec{k}_2 + \vec{k})}{E_\pi(k_1) + E_\pi(k_2) + E_\sigma(k)} \right] + \text{H.c.} \right). \end{aligned} \quad (2.15)$$

By using Eq. (2.11), Eq. (2.10) can be written as

$$H' = H_0 + H_I', \quad (2.16)$$

with

$$H_I' = H_I^P + [H_I^P, iS] + \frac{1}{2} [H_I^Q, iS] + \text{higher-order terms.} \quad (2.17)$$

Since  $H_I^P$ ,  $H_I^Q$ , and  $S$  are all of the first order in the coupling constant  $g_{\sigma\pi\pi}$ , all processes included in the second and third terms of the  $H_I'$  are of the order of  $g_{\sigma\pi\pi}^2$ . But some of them are "real processes," such as the  $\sigma$ -exchange  $\pi\pi$  interaction and  $\pi$ -exchange  $\pi\pi \rightarrow \sigma\sigma$  transition, as illustrated in the upper half of Fig. 2. The other processes are "virtual processes." An example is the emission of two  $\sigma$  mesons by a pion illustrated in the lower half of Fig. 2. We therefore rewrite Eq. (2.17) as

$$H'_I = H_I^P + H_I'^P + H_I'^Q + \sum_{n \geq 3} O(g_{\sigma\pi\pi}^n), \quad (2.18)$$

where

$$H_I'^P = ([H_I^P, iS] + \frac{1}{2}[H_I^Q, iS])^P, \quad (2.19)$$

$$H_I'^Q = ([H_I^P, iS] + \frac{1}{2}[H_I^Q, iS])^Q. \quad (2.20)$$

In the above two definitions,  $H_I'^P(H_I'^Q)$  is obtained by evaluating the commutators using Eqs. (2.7), (2.8), and (2.15) and keeping only the real (virtual) processes in the results.

The next step is to perform a second unitary transformation to eliminate  $H_I'^Q$ . In this paper we only consider the effective Hamiltonian up to second order in the coupling constant, and so we do not need to consider the second unitary transformation. The effective Hamiltonian is then obtained by dropping  $H_I'^Q$  and higher-order terms in Eq. (2.18):

$$H_{\text{eff}} = H + H_I^P + H_I'^P, \quad (2.21)$$

where  $H_I^P$  is defined by Eq. (2.7), and  $H_I'^P$  can be calculated from Eq. (2.19) by using the solution Eq. (2.15) for  $S$ . Note that both  $H_I^Q$  and  $iS$  contain a virtual  $\pi \leftrightarrow \pi\sigma$  vertex. They are included in  $H_I'^P$  of the effective Hamiltonian  $H_{\text{eff}}$  in a commutator form, as seen in the second term of Eq. (2.19). Consequently, the effect due to the  $\pi \leftrightarrow \pi\sigma$  vertex can give a  $\pi \rightarrow \pi\sigma \rightarrow \pi$  loop correction to the pion mass operator of the effective Hamiltonian  $H_{\text{eff}}$ . Furthermore, one can see by performing some straightforward derivations that the matrix element of  $H_{\text{eff}}$  between a  $\pi$  and a  $\pi\sigma$  state vanishes. This simplification is the consequence of the SKO method defined by Eq. (2.11) in operator form, and is not due to the choice of a model space in which some virtual states are omitted. If we choose the pion mass in  $H_0$  as the physical mass, the loop correction should be dropped from  $H_I'^P$  in order to avoid double counting. A similar situation will be encountered in the derivation of the  $\pi N$  effective Hamiltonian. The virtual  $N \leftrightarrow \pi N$  process can give a  $N \rightarrow \pi N \rightarrow N$  loop correction to the nucleon mass operator. The matrix element of the constructed effective Hamiltonian between an  $N$  state and a  $\pi N$  state vanishes. In our model we choose the physical masses for  $N$  and  $\pi$  in the free Hamiltonian and hence the loop corrections in the effective Hamiltonian are also dropped. This phenomenological procedure saves us from facing the complicated mass renormalization problem in solving the  $\pi N$  scattering problems.

Because of Eq. (2.14), Eqs. (2.12) and (2.13) lead to the simple relation

$$\langle f|iS|i\rangle = \frac{-1}{E_f - E_i} \langle f|H_I^Q|i\rangle, \quad (2.22)$$

where  $|f\rangle$  and  $|i\rangle$  are two eigenstates of  $H_0$ . With the above relation, the calculation of  $H_I'^P$ , Eq. (2.19), becomes

$$\begin{aligned} \langle f|H_I'^P|i\rangle = \sum_n \left\{ \langle f|H_I^P|n\rangle \langle n|H_I^Q|i\rangle \frac{1}{E_i - E_n} \right. \\ \left. - \langle f|H_I^Q|n\rangle \langle n|H_I^P|i\rangle \frac{1}{E_n - E_f} \right. \\ \left. + \langle f|H_I^Q|n\rangle \langle n|H_I^Q|i\rangle \frac{1}{2} \left[ \frac{1}{E_i - E_n} - \frac{1}{E_n - E_f} \right] \right\}. \end{aligned} \quad (2.23)$$

The calculation of the matrix element of  $H_I'^P$  therefore has a very simple rule. For a given choice of basis states  $|i\rangle$  and  $|f\rangle$ , the allowed intermediate state  $n$  is determined by the operator structure of  $O_n$  in Eqs. (2.12) and (2.13). The denominator in Eq. (2.23) can easily be written down by using eigenvalues of the free Hamiltonian  $H_0$ .

Evaluating  $H_I^P$  and  $H_I'^P$  explicitly within the coupled  $\pi\pi \oplus \sigma$  space, Eq. (2.21) can be cast into the following more familiar form for  $\pi\pi$  scattering:

$$H_{\text{eff}}^{\pi\pi} = H_0 + f_{\sigma \leftrightarrow \pi\pi} + V_{\pi\pi}. \quad (2.24)$$

Here  $H_0$  is the free Hamiltonian operator for  $\pi$  and  $\sigma$  mesons. The second term describes the  $\sigma \leftrightarrow \pi\pi$  transition with the matrix element

$$\langle \vec{k}_1 \vec{k}_2 | f_{\pi\pi, \sigma} | \vec{k} \rangle = \frac{\sqrt{2} g_{\sigma\pi\pi}}{\sqrt{(2\pi)^3 8 E_{\pi}(k_1) E_{\pi}(k_2) E_{\sigma}(k)}}. \quad (2.25)$$

The  $\pi\pi$  potential  $V_{\pi\pi}$  is obtained by using Eq. (2.23) to calculate  $H_I'^P$  between two  $\pi\pi$  states. For  $|i\rangle = |\vec{k}_{i1} \vec{k}_{i2}\rangle = \sqrt{\frac{1}{2}} [a_{\vec{k}_{i1}}^\dagger a_{\vec{k}_{i2}}^\dagger] |0\rangle$  and  $\langle f| = \langle \vec{k}_{f1} \vec{k}_{f2} | = \langle 0 | [a_{\vec{k}_{f1}} a_{\vec{k}_{f2}}] \sqrt{\frac{1}{2}}$  the possible intermediate states in Eq. (2.23) are  $|\pi\pi\sigma\rangle$  and  $|\pi\pi\pi\pi\sigma\rangle$  states. Inserting these intermediate states into Eq. (2.23) and carrying out straightforward operator algebra, we obtain

$$V_{\pi\pi} = V_{\pi\pi}^s + V_{\pi\pi}^t, \quad (2.26)$$

with the following the matrix elements between two  $\pi\pi$  states:

$$\begin{aligned} \langle \vec{k}_{f1} \vec{k}_{f2} | V_{\pi\pi}^s | \vec{k}_{i1} \vec{k}_{i2} \rangle = \frac{g_{\sigma\pi\pi}^2}{(2\pi)^3} \frac{1}{\sqrt{2 E_{\pi}(k_{f1})}} \frac{1}{\sqrt{2 E_{\pi}(k_{f2})}} \\ \times \frac{1}{\sqrt{2 E_{\pi}(k_{i1})}} \frac{1}{\sqrt{2 E_{\pi}(k_{i2})}} \\ \times [D_{\sigma}^{(-)}(k_{i1} + k_{i2}) + D_{\sigma}^{(-)}(k_{f1} + k_{f2})], \end{aligned} \quad (2.27)$$

$$\begin{aligned}
\langle \vec{k}_{f1} \vec{k}_{f2} | V_{\pi\pi}^t | \vec{k}_{i1} \vec{k}_{i2} \rangle &= \frac{g_{\sigma\pi\pi}^2}{(2\pi)^3} \frac{1}{\sqrt{2E_\pi(k_{f1})}} \frac{1}{\sqrt{2E_\pi(k_{f2})}} \\
&\times \frac{1}{\sqrt{2E_\pi(k_{i1})}} \frac{1}{\sqrt{2E_\pi(k_{i2})}} \\
&\times [D_\sigma(k_{i1}-k_{f2}) + D_\sigma(k_{i2}-k_{f1}) \\
&+ D_\sigma(k_{i1}-k_{f1}) + D_\sigma(k_{i2}-k_{f2})],
\end{aligned} \tag{2.28}$$

where

$$D_\sigma(k) = \frac{1}{k^2 - m_\sigma^2} = D^{(+)}(k) + D^{(-)}(k), \tag{2.29}$$

with

$$D_\sigma^{(\pm)}(k) = \frac{1}{2E_\sigma(k)} \frac{\pm 1}{k_0 \mp E_\sigma(k)}. \tag{2.30}$$

This completes the illustration of the SKO method in deriving an effective Hamiltonian from a model Lagrangian of relativistic quantum field theory. The extension of the method to consider more realistic Lagrangians is straightforward and will not be further detailed. In the following sections, we will simply write down the starting Lagrangians and the resulting effective Hamiltonians up to second order in the coupling constants for  $\pi N$  scattering and the  $\gamma N \rightarrow \pi N$  reaction.

### III. $\pi$ - $N$ SCATTERING

We start with the following commonly assumed [17] Lagrangian for  $N, \Delta, \pi$ , and  $\rho$  fields:

$$L(x) = L_0(x) + L_I(x), \tag{3.1}$$

where  $L_0(x)$  is the usual noninteracting Lagrangian, and the interaction is taken to be

$$L_I(x) = L_{\pi NN}(x) + L_{\pi N\Delta}(x) + L_{\rho NN}(x) + L_{\rho\pi\pi}(x), \tag{3.2}$$

with (in the convention of Bjorkin and Drell [52])

$$L_{\pi NN}(x) = -\frac{f_{\pi NN}}{m_\pi} \bar{\psi}_N(x) \gamma_5 \gamma_\mu \vec{\tau} \psi_N(x) \partial^\mu \cdot \vec{\phi}_\pi(x), \tag{3.3}$$

$$L_{\pi N\Delta} = \frac{f_{\pi N\Delta}}{m_\pi} \bar{\psi}_\Delta^\mu(x) \vec{T} \psi_N(x) \cdot \partial_\mu \vec{\phi}_\pi(x) + [\text{H.c.}], \tag{3.4}$$

$$\begin{aligned}
L_{\rho NN}(x) &= g_{\rho NN} \bar{\psi}_N(x) \frac{\vec{\tau}}{2} \cdot \left[ \gamma_\mu \vec{\phi}_\rho^\mu(x) - \frac{\kappa_\rho}{2m_N} \sigma_{\mu\nu} \partial^\nu \vec{\phi}_\rho^\mu(x) \right] \\
&\times \psi_N(x),
\end{aligned} \tag{3.5}$$

$$L_{\rho\pi\pi}(x) = g_{\rho\pi\pi} (\vec{\phi}_\pi \times \partial_\mu \vec{\phi}_\pi) \cdot \vec{\phi}_\rho^\mu. \tag{3.6}$$

Here  $\vec{T}$  is a  $N \rightarrow \Delta$  isospin transition operator defined by the reduced matrix element [54]  $\langle \frac{3}{2} || T || \frac{1}{2} \rangle = -\langle \frac{1}{2} || T^\dagger || \frac{3}{2} \rangle = 2$ . By using the standard canonical quantization, a Hamiltonian can be derived from the above Lagrangian except the term involving the  $\Delta$  field. The difficulty of quantizing the  $\Delta$  field is well known, as discussed, for example, in Refs. [55] and [56]. As part of our phenomenology, we take the simplest prescription by imposing the anticommutation relation

$$\{\Delta_p^-, \Delta_{p'}^\dagger\} = \delta(\vec{p} - \vec{p}'), \tag{3.7}$$

where  $\Delta_p^{\pm}$  ( $\Delta_p^\dagger$ ) is the annihilation (creation) operator for a  $\Delta$  state. This choice then leads [55] to the  $\Delta$  propagator given later in Eq. (3.18). The alternative approaches proposed in Ref. [56] will not be considered.

Following the procedure described in Sec. II, the next step is to decompose the resulting Hamiltonian into a  $H_I^P$  for ‘‘physical processes’’ and a  $H_I^Q$  for ‘‘virtual processes.’’ From Eqs. (3.3)–(3.6), it is clear that the real processes in this case are  $\Delta \leftrightarrow \pi N$  and  $\rho \leftrightarrow \pi\pi$  transitions which can take place in free space (because  $m_\Delta > m_N + m_\pi$  and  $m_\rho > 2m_\pi$ ). The virtual processes are  $N \leftrightarrow \pi N$ ,  $N \leftrightarrow \rho N$ ,  $N \leftrightarrow \pi\Delta$ , and  $\pi \leftrightarrow \pi\rho$  transitions. These virtual processes can be eliminated by introducing a unitary transformation operator  $S$  which can be determined by using the similar method in obtaining the solution Eqs. (2.13) and (2.14). Here, we of course encounter a much more involved task to account for the Dirac spin structure, isospin, and also the antiparticle components of  $N$  and  $\Delta$ . To see the main steps, we present in the Appendix an explicit derivation of the potential due to the  $L_{\pi NN}$  term, Eq. (3.3).

For practical applications, it is sufficient to present our results in the coupled  $\pi N \oplus \Delta$  subspace in which the  $\pi N$  scattering problem will be solved. The resulting effective Hamiltonian then takes the form

$$H_{\text{eff}}^{\pi N} = H_0 + \Gamma_{\Delta \leftrightarrow \pi N} + v_{\pi N}, \tag{3.8}$$

where  $H_0$  is the free Hamiltonian for  $\pi$ ,  $N$ , and  $\Delta$ . Note that  $\Gamma_{\Delta \leftrightarrow \pi N}$  [Figs. 3(a) and 3(b)] is the only vertex interaction in the constructed effective Hamiltonian. Our model is therefore distinctively different from the previous meson-exchange  $\pi N$  models [12–14, 19] which all involve a bare nucleon state  $N_0$  and a  $N_0 \leftrightarrow \pi N$  vertex.

The  $\pi N$  potential  $v_{\pi N}$  in Eq. (3.8) is found to be

$$v_{\pi N} = v_{N_D} + v_{N_E} + v_\rho + v_{\Delta_D} + v_{\Delta_E}, \tag{3.9}$$

where  $v_{N_D}$  is the direct nucleon pole term [Fig. 3(c)],  $v_{N_E}$  the nucleon-exchange term [Fig. 3(d)],  $v_\rho$  the  $\rho$ -exchange term [Fig. 3(e)],  $v_{\Delta_D}$  the interaction due to the anti- $\Delta$  component of the  $\Delta$  propagation [Fig. 3(f)], and  $v_{\Delta_E}$  the  $\Delta$ -exchange term [Fig. 3(g)]. To simplify the presentation, we will only give the matrix element of  $v_{\pi N}$  in the  $\pi N$  center-of-mass

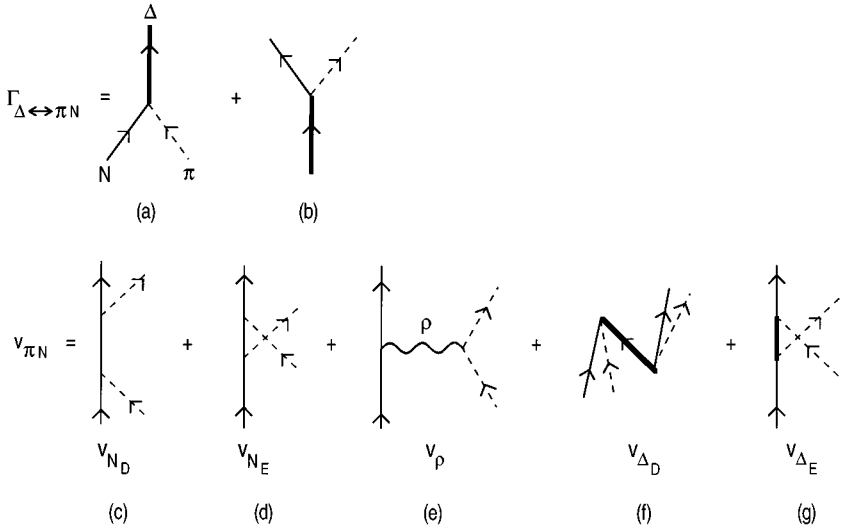


FIG. 3. Graphical representation of the interactions of the effective Hamiltonian, Eq. (3.8), in the coupled  $\pi N \oplus \Delta$  space.

frame. The initial and final four-momenta  $k^\mu, k'^\mu$  for pions and  $p^\mu, p'^\mu$  for the nucleons in Fig. 3 are therefore defined as

$$k^\mu = (E_\pi(k), \vec{k}), \quad (3.10)$$

$$p^\mu = (E_N(k), -\vec{k}),$$

$$k'^\mu = (E_\pi(k'), \vec{k}'),$$

$$p'^\mu = (E_N(k'), -\vec{k}').$$

In terms of these variables, the matrix element of each term of Eq. (3.9) between two  $\pi N$  states can be written as

$$\langle \vec{k}' i', m'_s m'_\tau | v_\alpha | \vec{k} i, m_s, m_\tau \rangle = \frac{1}{(2\pi)^3} \frac{1}{\sqrt{2E_\pi(k')}} \sqrt{\frac{m_N}{E_N(k')}} \frac{1}{\sqrt{2E_\pi(k)}} \sqrt{\frac{m_N}{E_N(k)}} \bar{u}_{-\vec{k}', m'_s, m'_\tau} I_\alpha(\vec{k}' i', \vec{k} i) u_{-\vec{k}, m_s, m_\tau}, \quad (3.11)$$

where  $u_{\vec{p}, m_s, m_\tau}$  is the Dirac spinor,  $m_s$  and  $m_\tau$  are the nucleon spin and isospin quantum numbers, and  $i$  and  $i'$  are the pion isospin components. The interaction mechanisms are contained in the functions  $I_\alpha(\vec{k}' i', \vec{k} i)$ . After performing lengthy derivations, we find that these functions can be written in the concise forms

$$I_{N_D}(\vec{k}' i', \vec{k} i) = \left( \frac{f_{\pi NN}}{m_\pi} \right)^2 \tau_i \gamma^5 \mathbf{k}' \cdot \frac{1}{2} [S_N(p+k) + S_N(p'+k')] \times \tau_i \gamma^5 \mathbf{k}, \quad (3.12)$$

$$I_{N_E}(\vec{k}' i', \vec{k} i) = \left( \frac{f_{\pi NN}}{m_\pi} \right)^2 \tau_i \gamma^5 \mathbf{k}' \cdot \frac{1}{2} [S_N(p-k') + S_N(p'-k)] \times \tau_i \gamma^5 \mathbf{k}', \quad (3.13)$$

$$I_\rho(\vec{k}' i', \vec{k} i) = \frac{i g_{\rho NN} g_{\rho \pi \pi}}{4} \epsilon_{ii'k\tau} \left\{ \left[ \gamma_\mu - \frac{\kappa_\rho}{2m_N} i \sigma_{\mu\nu} (p-p')^\nu \right] \times [D_\rho^{\mu\lambda}(p-p')(k+k')_\lambda] + [(p-p') \leftrightarrow (k'-k)] \right\}, \quad (3.14)$$

$$I_{\Delta_D}(\vec{k}' i', \vec{k} i) = \left( \frac{f_{\pi N \Delta}}{m_\pi} \right)^2 T_i^\dagger k_\mu \cdot \frac{1}{2} [S_\Delta^{\mu\nu}(p+k) + S_\Delta^{\mu\nu}(p'+k') - S_\Delta^{(+)\mu\nu}(p+k) - S_\Delta^{(+)\mu\nu}(p'+k')] T_i k_\nu, \quad (3.15)$$

$$I_{\Delta E}(\vec{k}' i', \vec{k} i) = \left( \frac{f_{\pi N \Delta}}{m_\pi} \right)^2 T_i^\dagger k_\mu \cdot \frac{1}{2} [S_\Delta^{\mu\nu}(p-k') + S_\Delta^{\mu\nu}(p'-k)] T_i k'_\nu. \quad (3.16)$$

The propagators in the above equations are defined as

$$S_N(p) = \frac{1}{\not{p} - m_N}, \quad (3.17)$$

$$S_\Delta^{\mu\nu}(p) = \frac{1}{3(\not{p} - m_\Delta)} \left[ 2 \left( -g^{\mu\nu} + \frac{p^\mu p^\nu}{m_\Delta^2} \right) + \frac{\gamma^\mu \gamma^\nu - \gamma^\nu \gamma^\mu}{2} - \frac{p^\mu \gamma^\nu - p^\nu \gamma^\mu}{m_\Delta} \right], \quad (3.18)$$

$$D_{\rho}^{\mu\nu}(p) = -\frac{g^{\mu\nu} - p^{\mu}p^{\nu}/m_{\rho}^2}{p^2 - m_{\rho}^2}. \quad (3.19)$$

In Eq. (3.15), we also have introduced a propagator

$$S_{\Delta}^{(+)\mu\nu}(p) = \frac{m_{\Delta}}{E_{\Delta}(p)} \frac{\omega_{\rho}^{\mu} \bar{\omega}_{\rho}^{\nu}}{p_0 - E_{\Delta}(p)}, \quad (3.20)$$

where  $\omega_{\rho}^{\mu}$  is the Rarita-Schwinger spinor (as explicitly defined in Ref. [17]). In the  $\Delta$  rest frame, this propagator reduces to the simple form

$$S^{(+)\mu\nu}(p) \xrightarrow{\vec{p} \rightarrow 0} \frac{1 + \gamma^0}{6} (3\delta^{ij} - \sigma^i \sigma^j) \frac{1}{p_0 - m_{\Delta}} \quad (3.21)$$

for  $i, j = 1, 2, 3$ . The other elements involving time components vanish in this special frame,  $S^{(+)\mu 0} = S^{(+)\mu 0} = 0$ . The appearance of this propagator in Eq. (3.15) is to remove the  $\pi N \rightarrow \Delta \rightarrow \pi N$  mechanism which can be generated by the vertex interaction  $\Gamma_{\Delta \leftrightarrow \pi N}$  of the effective Hamiltonian Eq. (3.8). This comes about naturally in our derivations.

We note that the above expressions are remarkably similar to those derived from using Feynman rules. The only differences are in the propagators of the intermediate particles. These propagators are evaluated by using the momenta of the external particles which are restricted on their mass shell, as defined in Eq. (3.10). For the off-energy-shell dynamics [ $E_N(k) + E_{\pi}(k) \neq E_N(k') + E_{\pi}(k')$ ], these propagators can have two possible forms, depending on which set of external momenta is used. The propagators in Eqs. (3.12)–(3.16) are the average of these two possible forms of propagators. More details can be seen in the Appendix where the derivation of  $v_N = v_{N_D} + v_{N_E}$  is given explicitly.

In the  $\pi N$  center-of-mass frame, the  $\Delta$  in the vertex interaction  $\Gamma_{\Delta \leftrightarrow \pi N}$  is at rest. In this particular frame, the Rarita-Schwinger spinors reduce to a simple form such that the matrix element of the vertex interaction  $\Gamma_{\Delta \leftrightarrow \pi N}$  takes the familiar form

$$\begin{aligned} \langle \Delta | \Gamma_{\Delta \leftrightarrow \pi N} | \vec{k} i \rangle &= -\frac{f_{\pi N \Delta}}{m_{\pi}} \frac{i}{\sqrt{(2\pi)^3} \sqrt{2E_{\pi}(k)}} \frac{1}{\sqrt{2E_N(k)}} \\ &\times \sqrt{\frac{E_N(k) + m_N}{2E_N(k)}} \vec{S} \cdot \vec{k} T_i. \end{aligned} \quad (3.22)$$

Here  $\vec{S}$  is a  $N \rightarrow \Delta$  transition spin operator. It is defined by the same reduced matrix element as the transition isospin operator  $T$ .

Because of the absence of a  $\pi N \leftrightarrow N$  vertex in the effective Hamiltonian, Eq. (3.8), it is straightforward to derive the  $\pi N$  scattering equations in the coupled  $\pi N \oplus \Delta$  space. The derivation procedure is similar to that given in Ref. [23] for the more complicated  $\pi NN$  problem. The essential idea is to apply the standard projection operator technique of nuclear reaction theory [3]. The resulting scattering amplitude can be cast into the form

$$T_{\pi N}(E) = t_{\pi N}(E) + \bar{\Gamma}_{\Delta \rightarrow \pi N}(E) G_{\Delta}(E) \bar{\Gamma}_{\pi N \rightarrow \Delta}(E). \quad (3.23)$$

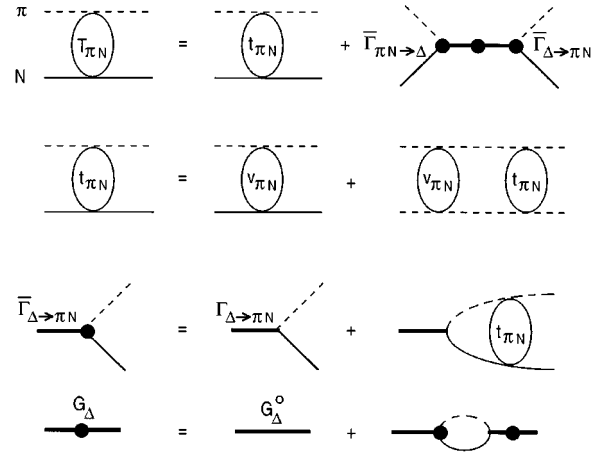


FIG. 4. Graphical representation of scattering equations defined by Eqs. (3.23)–(3.30).

The first term is the nonresonant amplitude determined only by the  $\pi N$  potential:

$$t_{\pi N}(E) = v_{\pi N} + v_{\pi N} G_{\pi N}(E) t_{\pi N}(E), \quad (3.24)$$

with

$$G_{\pi N}(E) = \frac{P_{\pi N}}{E - E_N(k) - E_{\pi}(k) + i\epsilon}, \quad (3.25)$$

where  $P_{\pi N}$  is the projection operator for the  $\pi N$  subspace. The second term of Eq. (3.23) is the resonant term determined by the dressed  $\Delta$  propagator and the dressed vertex functions. They are defined by

$$\begin{aligned} G_{\Delta}(E) &= G_{\Delta}^0(E) + G_{\Delta}^0(E) \Sigma_{\Delta}(E) G_{\Delta}(E) \\ &= \frac{P_{\Delta}}{E - m_{\Delta} - \Sigma_{\Delta}(E)}, \end{aligned} \quad (3.26)$$

with

$$G_{\Delta}^0(E) = \frac{P_{\Delta}}{E - m_{\Delta}} \quad (3.27)$$

and

$$\bar{\Gamma}_{\pi N \rightarrow \Delta}(E) = \Gamma_{\pi N \rightarrow \Delta} [1 + G_{\pi N}(E) t_{\pi N}(E)], \quad (3.28)$$

$$\bar{\Gamma}_{\Delta \rightarrow \pi N}(E) = [1 + G_{\pi N}(E) t_{\pi N}(E)] \Gamma_{\Delta \rightarrow \pi N}, \quad (3.29)$$

where  $P_{\Delta}$  is the projection operator for the  $\Delta$  state, and the  $\Delta$  self-energy is defined by

$$\Sigma_{\Delta}(E) = \Gamma_{\pi N \rightarrow \Delta} G_{\pi N}(E) \bar{\Gamma}_{\Delta \rightarrow \pi N}(E). \quad (3.30)$$

Equations (3.23)–(3.30) are illustrated in Fig. 4. These equations are solved in partial-wave representation. To find the solution for the integral equation (3.24), it is necessary to regularize the  $\pi N$  potential by introducing a form factor for each vertex in Eqs. (3.12)–(3.16). In this work, we choose



$$[I_{ND} + I_{NE}](\vec{k}' i', \vec{k} i) \rightarrow [I_{ND} + I_{NE}](\vec{k}' i', \vec{k} i) \\ \times F_{\pi NN}(\vec{k}') F_{\pi NN}(\vec{k}), \quad (3.31)$$

$$I_\rho(\vec{k}' i', \vec{k} i) \rightarrow I_\rho(\vec{k}' i', \vec{k} i) F_{\rho NN}(\vec{k} - \vec{k}') F_{\rho \pi \pi}(\vec{k} - \vec{k}'), \quad (3.32)$$

with

$$F_{\pi NN}(\vec{k}) = \left( \frac{\Lambda_{\pi NN}^2}{\Lambda_{\pi NN}^2 + \vec{k}^2} \right)^2, \quad (3.33)$$

$$F_{\rho NN}(\vec{k} - \vec{k}') = F_{\rho \pi \pi}(\vec{k} - \vec{k}'), \quad (3.34) \\ = \left( \frac{\Lambda_\rho^2}{\Lambda_\rho^2 + (\vec{k} - \vec{k}')^2} \right)^2. \quad (3.35)$$

For  $\pi N \Delta$  vertex with an external pion momentum  $\vec{k}$ , we choose

$$F_{\pi N \Delta}(\vec{k}) = \left( \frac{\Lambda_{\pi N \Delta}^2}{\Lambda_{\pi N \Delta}^2 + \vec{k}^2} \right)^2. \quad (3.36)$$

We have also tried other parametrizations of form factors, but they do not give better fits to the  $\pi N$  scattering phase shifts.

#### IV. PION PHOTOPRODUCTION

To proceed, we need to first extend the Lagrangian, Eq. (3.1), to include  $\omega$  meson coupling which is known [4,17] to play an important role in pion photoproduction. We choose the following rather conventional form (with  $\kappa_\omega \sim 0$ )

$$L_{\omega NN} = g_{\omega NN} \bar{\psi}_N(x) \left[ \gamma_\mu \phi_\omega^\mu(x) - \frac{\kappa_\omega}{2m_N} \sigma_{\mu\nu} \partial^\nu \phi_\omega^\mu(x) \right] \psi_N(x). \quad (4.1)$$

Following the approach of Ref. [17], the pion photoproduction mechanisms are defined by the hadronic Lagrangians defined by Eqs. (3.1) and (4.1) and the electromagnetic interaction Lagrangians

$$L_{\text{em}} = L_{\gamma NN} + L_{\gamma \pi \pi} + L_{\gamma \pi NN} + L_{\gamma \rho \pi} + L_{\gamma \omega \pi} + L_{\gamma N \Delta}, \quad (4.2)$$

with

$$L_{\gamma NN} = -e \bar{\psi}_N(x) \left[ \hat{e} \vec{A}(x) - \frac{\hat{\kappa}}{2m_N} \sigma_{\mu\nu} [\partial^\nu A^\mu(x)] \right] \psi_N(x), \quad (4.3)$$

$$L_{\gamma \pi NN} = -\frac{ef_{\pi NN}}{m_\pi} \bar{\psi}_N(x) \gamma_5 \vec{A}(x) [\vec{\tau} \times \vec{\phi}_\pi(x)]_3 \psi_N(x), \quad (4.4)$$

$$L_{\gamma \pi \pi} = e [\partial^\mu \vec{\phi}_\pi(x) \times \vec{\phi}_\pi(x)]_3 A_\mu(x), \quad (4.5)$$

$$L_{\rho \pi \gamma} = \frac{g_{\rho \pi \gamma}}{m_\pi} \epsilon_{\alpha\beta\gamma\delta} [\partial^\alpha A^\beta(x)] \vec{\phi}_\pi(x) \cdot [\partial^\gamma \vec{\phi}_\rho^\delta(x)], \quad (4.6)$$

$$L_{\omega \pi \gamma} = \frac{g_{\omega \pi \gamma}}{m_\pi} \epsilon_{\alpha\beta\gamma\delta} [\partial^\alpha A^\beta(x)] \phi_\pi^3(x) [\partial^\gamma \phi_\omega^\delta(x)], \quad (4.7)$$

$$L_{\gamma N \Delta} = ie \bar{\psi}_\Delta^\mu T_3 \Gamma_{\mu\nu} A^\nu(x) \psi_N(x) + [\text{H.c.}]. \quad (4.8)$$

Here  $\hat{e} = (1 + \tau_3)/2$ ,  $\hat{\kappa} = (\kappa_p + \kappa_n)/2 + (\kappa_p - \kappa_n)\tau_3/2$ . The  $\gamma N \Delta$  coupling in Eq. (4.8) is

$$\Gamma_{\mu\nu} = (G_M K_{\mu\nu}^M + G_E K_{\mu\nu}^E), \quad (4.9)$$

as defined in Eqs. (2.10b) and (2.10c) of Ref. [17]. Its matrix element between an  $N$  with momentum  $p$  and a  $\Delta$  with momentum  $p_\Delta$  can be written explicitly as

$$\langle \Delta(p_\Delta) | \Gamma_{\mu\nu} | N(p) \rangle = (G_M - G_E) \left[ \frac{3}{(m_\Delta + m_N)^2 - q^2} \frac{m_\Delta + m_N}{2m_N} \epsilon_{\mu\nu\alpha\beta} P^\alpha q^\beta \right] \\ + G_E i \gamma^5 \left[ \frac{6}{[(m_\Delta + m_N)^2 - q^2][(m_\Delta - m_N)^2 - q^2]} \frac{m_\Delta + m_N}{m_N} \epsilon_{\mu\lambda\alpha\beta} P^\alpha q^\beta \epsilon_{\nu\gamma\delta}^\lambda P^\gamma q^\delta \right], \quad (4.10)$$

with  $P = (p + p_\Delta)/2$  and  $p_\Delta = p + q$ .

By applying the usual canonical quantization procedure, we can obtain from the above Lagrangians an electromagnetic interaction Hamiltonian  $H_{\text{em}}$ . In this work, we will treat the electromagnetic field as an external classical field, and hence the electromagnetic interaction  $H_{\text{em}}$  can be neglected in constructing the unitary transformation operator  $S$ . The effective Hamiltonian for describing pion photopro-

duction is therefore a simple extension of the effective Hamiltonian of the form of Eq. (2.21):

$$H_{\text{eff}} \rightarrow H_{\text{eff}} + H_{\text{eff}}^{\text{em}} \\ = H_0 + H_I^P + H_I^{\prime P} + H_{\text{eff}}^{\text{em}}, \quad (4.11)$$

with

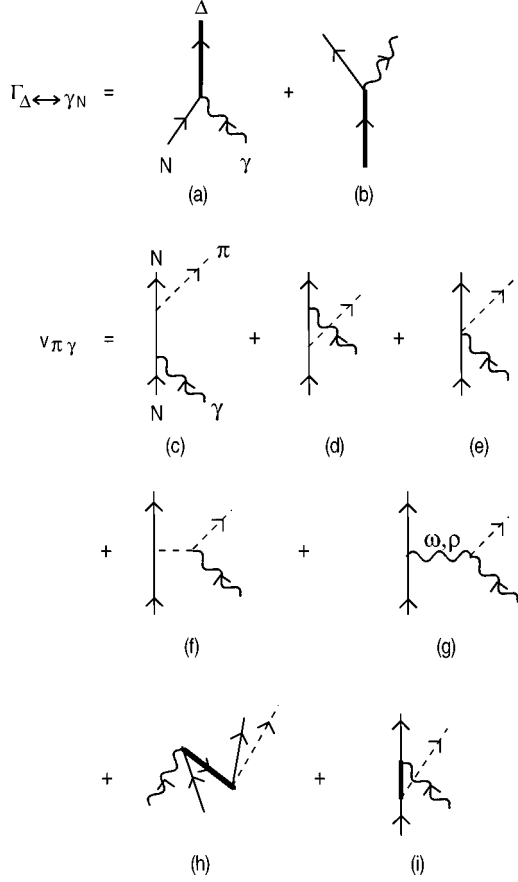


FIG. 5. Graphical representation of the effective interactions  $\Gamma_{\Delta \leftrightarrow \gamma N}$  and  $v_{\pi\gamma}$  of Eq. (4.13).

$$H_{\text{eff}}^{\text{em}} = H_{\text{em}} + [H_{\text{em}}, iS]. \quad (4.12)$$

By evaluating  $H_{\text{eff}}^{\text{em}}$  in the coupled  $\Delta \oplus \pi N \oplus \gamma N$  subspace, we obtain an extension of Eq. (3.8):

$$H_{\text{eff}}^{\pi \rightarrow \gamma} = H_0 + \Gamma_{\Delta \leftrightarrow \pi N} + v_{\pi N} + \Gamma_{\Delta \leftrightarrow \gamma N} + v_{\pi\gamma}, \quad (4.13)$$

where  $\Gamma_{\Delta \leftrightarrow \pi N}$  and  $v_{\pi N}$  have already been given in Eqs. (3.11)–(3.22). The resonant and nonresonant electromagnetic interactions are, respectively, described by  $\Gamma_{\Delta \leftrightarrow \gamma N}$  and  $v_{\pi\gamma}$ , and are illustrated in Fig. 5. We again omit the details of the derivation of these two terms, and simply present our

results in the center-of-mass frame. The momenta variables  $q^\mu$  for the photon,  $p^\mu$  for the initial nucleon,  $k^\mu$  for the pion, and  $p'^\mu$  for the final nucleon, in Fig. 5, are therefore

$$q^\mu = (q, \vec{q}),$$

$$p^\mu = (E_N(q), -\vec{q}),$$

$$k^\mu = (E_\pi(k), \vec{k}),$$

$$p'^\mu = (E_N(k), -\vec{k}). \quad (4.14)$$

In terms of these variables, expression (4.10) becomes very simple. The matrix element of the  $\Gamma_{\Delta \leftrightarrow \gamma N}$  vertex can then be expressed in terms of the spin and isospin  $N \rightarrow \Delta$  transition-operators  $S$  and  $T$  introduced in Sec. III. At the resonance energy,  $m_\Delta = E_N(q) + q$ , Eq. (4.10) leads to

$$\begin{aligned} \langle \Delta | \Gamma_{\gamma N \rightarrow \Delta} | \vec{q} \lambda \rangle &= -\frac{e}{(2\pi)^{3/2}} \sqrt{\frac{E_N(q) + m_N}{2E_N(q)}} \\ &\times \frac{1}{\sqrt{2q}} \frac{3m_\Delta}{2m_N(m_\Delta + m_N)} T_3 [iG_M \vec{S} \times \vec{q} \cdot \vec{\epsilon}_\lambda \\ &+ G_E (\vec{S} \cdot \vec{\epsilon}_\lambda \vec{\sigma} \cdot \vec{q} + \vec{S} \cdot \vec{q} \vec{\sigma} \cdot \vec{\epsilon}_\lambda)], \end{aligned} \quad (4.15)$$

where  $\vec{\epsilon}_\lambda$  is the photon polarization vector. The matrix element of the nonresonant interaction  $v_{\pi\gamma}$  can be written as

$$\begin{aligned} \langle \vec{k} i, m'_s m'_\tau | v_{\pi\gamma} | \vec{q} \lambda, m_s m_\tau \rangle &= \frac{1}{(2\pi)^3} \frac{1}{\sqrt{2E_\pi(k)}} \frac{1}{\sqrt{2q}} \sqrt{\frac{m_N}{E_N(k)}} \sqrt{\frac{m_N}{E_N(q)}} \\ &\times \bar{u}_{-k m'_s m'_\tau} \left[ \sum_\alpha I_\alpha^{\pi\gamma}(\vec{k} i, \vec{q} \lambda) \right] u_{-k m_s m_\tau}. \end{aligned} \quad (4.16)$$

The nonresonant pion photoproduction mechanisms are contained in  $I_N^{\pi\gamma}$  for the direct nucleon terms [Figs. 5(c), 5(d), and 5(e)],  $I_\pi^{\pi\gamma}$  for the pion pole term [Fig. 5(f)],  $I_{\rho, \omega}^{\pi\gamma}$  for the vector meson-exchange [Fig. 5(g)], and  $I_{\Delta D, \Delta E}^{\pi\gamma}$  for the direct and exchange  $\Delta$  terms [Figs. 5(h) and 5(i)]. Explicitly, we have

$$\begin{aligned} I_N^{\pi\gamma}(\vec{k} i, \vec{q} \lambda) &= \frac{ef_{\pi NN}}{m_\pi} \left[ i\tau_i \gamma^5 \mathbf{k} S_N(p' + k) \left( \hat{e} \cdot \hat{k}(\lambda) + i \frac{\hat{k}}{2m_N} \sigma_{\mu\nu} \epsilon(\lambda)^\mu q^\nu \right) + i \left( \hat{e} \cdot \hat{k}(\lambda) + i \frac{\hat{k}}{2m_N} \sigma_{\mu\nu} \epsilon(\lambda)^\mu q^\nu \right) \right. \\ &\left. \times S_N(p - k) \tau_i \gamma^5 \mathbf{k} - \epsilon_{ij3} \tau_j \gamma^5 \hat{k}(\lambda) \right], \end{aligned} \quad (4.17)$$

$$I_\pi^{\pi\gamma}(\vec{k} i, \vec{q} \lambda) = -\frac{ef_{\pi NN}}{m_\pi} \epsilon_{ij3} \tau_j \gamma^5 (\hat{p}' - \hat{p}) [(k + p - p') \cdot \epsilon(\lambda) D_\pi(p - p')], \quad (4.18)$$

$$I_{\rho}^{\pi\gamma}(\vec{k}i, \vec{q}\lambda) = \frac{g_{\rho NN} g_{\rho\pi\gamma}}{m_{\pi}} \frac{\tau_i}{2} \left[ \gamma_{\mu} - \frac{i\kappa_{\rho}}{2m_N} \sigma_{\mu\eta} (p-p')^{\eta} \right] \times D_{\rho}^{\mu\nu}(p-p') \epsilon_{\alpha\beta\gamma\nu} \epsilon^{\alpha}(\lambda) q^{\beta} (p-p')^{\gamma},$$

$$I_{\omega}^{\pi\gamma}(\vec{k}i, \vec{q}\lambda) = \frac{g_{\omega NN} g_{\omega\pi\gamma}}{m_{\pi}} \delta_{i,3} \left[ \gamma_{\mu} - \frac{i\kappa_{\omega}}{2m_N} \sigma_{\mu\eta} (p-p')^{\eta} \right] \times D_{\omega}^{\mu\nu}(p-p') \epsilon_{\alpha\beta\gamma\nu} \epsilon^{\alpha}(\lambda) q^{\beta} (p-p')^{\gamma} \quad (4.19)$$

$$I_{\Delta E}^{\pi\gamma}(\vec{k}i, \vec{q}\lambda) = \frac{ef_{\pi N\Delta}}{m_{\pi}} T_3^{\dagger} \Gamma_{\mu\delta}^{\dagger} \epsilon^{\delta}(\lambda) S_{\Delta}^{\mu\nu}(p-k) T_i k_{\nu}, \quad (4.20)$$

$$I_{\Delta D}^{\pi\gamma}(\vec{k}i, \vec{q}\lambda) = -\frac{ef_{\pi N\Delta}}{m_{\pi}} T_i^{\dagger} k_{\mu} [S_{\Delta}^{\mu\nu}(p'+k) - S^{(+)\mu\nu}(p'+k)] T_3 \Gamma_{\nu\delta} \epsilon^{\delta}(\lambda). \quad (4.21)$$

Here we observe again that the above expressions are very similar to the results derived by using Feynman rules. However, they have an important feature that the time components of the momenta in the propagators and strong interaction vertices are evaluated by using the external momenta of the final  $\pi N$  state. This is the consequence of applying the unitary transformation method defined in Eq. (4.12). In addition to including nonresonant  $\Delta$  terms [Figs. 5(h) and 5(i)], this is another feature which makes our model different from the model developed in Ref. [17].

It is straightforward to derive from the effective Hamiltonian, Eq. (4.13), the  $t$  matrix of pion photoproduction:

$$T_{\gamma\pi}(E) = t_{\gamma\pi}(E) + \bar{\Gamma}_{\Delta \leftrightarrow \pi N}(E) G_{\Delta}(E) \bar{\Gamma}_{\gamma N \rightarrow \Delta}(E), \quad (4.22)$$

where the nonresonant amplitude is defined by

$$t_{\gamma\pi}(E) = v_{\gamma\pi} + t_{\pi N}(E) G_{\pi N}(E) v_{\gamma\pi}. \quad (4.23)$$

The dressed  $\gamma N \leftrightarrow \Delta$  is defined by

$$\bar{\Gamma}_{\gamma N \rightarrow \Delta}(E) = \Gamma_{\gamma N \rightarrow \Delta} + \bar{\Gamma}_{\pi N \rightarrow \Delta}(E) G_{\pi N}(E) v_{\gamma\pi}. \quad (4.24)$$

In the above equations,  $G_{\Delta}$ ,  $\bar{\Gamma}_{\Delta \leftrightarrow \pi N}$ ,  $G_{\pi N}$ , and  $t_{\pi N}$  have been defined in Sec. III. The standard partial-wave decomposition is used to obtain the multipole amplitudes from  $T_{\gamma\pi}$  for the  $\gamma N \rightarrow \pi N$  reaction and from  $\bar{\Gamma}_{\Delta \leftrightarrow \pi N}$  for the dressed  $\Delta \leftrightarrow \pi N$  vertex. Equations (4.22)–(4.24) are illustrated in Fig. 6.

The  $K$ -matrix formulation of the  $\gamma N \rightarrow \pi N$  reaction is often used [4–7] in the analysis of data. Within our formulation, this can be obtained by replacing the  $\pi N$  free Green function  $G_{\pi N}$ , Eq. (3.25), by

$$G_{\pi N}(E) \rightarrow G_{\pi N}^P(E) = P \frac{P_{\pi N}}{E - E_N(k) - E_{\pi}(k)}, \quad (4.25)$$

where  $P$  means taking the principal-value part of the propagator. If this replacement is used in the calculations of Eqs. (3.23)–(3.30), all scattering quantities will be real numbers. These  $K$ -matrix quantities are defined by exactly the same Eqs. (3.23)–(3.30) with the changes

$$G_{\pi N} \rightarrow G_{\pi N}^P,$$

$$T_{\pi N} \rightarrow K_{\pi N},$$

$$t_{\pi N} \rightarrow k_{\pi N},$$

$$\bar{\Gamma}_{\Delta \leftrightarrow \pi N} \rightarrow \bar{\Gamma}_{\Delta \leftrightarrow \pi N}^k,$$

$$G_{\Delta} \rightarrow G_{\Delta}^P = \frac{P_{\Delta}}{E - m_{\Delta} - \Sigma_{\Delta}^k(E)}, \quad (4.26)$$

with

$$\Sigma_{\Delta}^k(E) = \Gamma_{\pi N \rightarrow \Delta} G_{\pi N}^P(E) \bar{\Gamma}_{\Delta \rightarrow \pi N}^k(E). \quad (4.27)$$

Note that the  $\Delta$  self-energy  $\Sigma_{\Delta}^k$  is now a real number, and the propagator  $G_{\Delta}^P$  has a pole at  $E = M_R = m_{\Delta} + \Sigma_{\Delta}^k(M_R)$ .

The corresponding  $K$  matrix for pion photoproduction can be obtained from Eqs. (4.22)–(4.24) by the same replacement, Eq. (4.25):

$$K_{\gamma\pi}(E) = k_{\gamma\pi}(E) + \bar{\Gamma}_{\Delta \rightarrow \pi N}^k(E) G_{\Delta}^P(E) \bar{\Gamma}_{\gamma N \rightarrow \Delta}^k(E), \quad (4.28)$$

with

$$k_{\gamma\pi} = v_{\gamma\pi} + k_{\pi N}(E) G_{\pi N}^P(E) v_{\gamma\pi}, \quad (4.29)$$

$$\bar{\Gamma}_{\gamma N \rightarrow \Delta}^k(E) = \Gamma_{\gamma N \rightarrow \Delta} + \bar{\Gamma}_{\pi N \rightarrow \Delta}^k(E) G_{\pi N}^P(E) v_{\gamma\pi}. \quad (4.30)$$

For the on-shell matrix elements [ $E = E_N(k_0) + E_{\pi}(k_0) = q + E_N(q)$ ], it is straightforward to find the following relation in each partial wave:

$$T_{\gamma\pi}(k_0, q) = [1 - i\pi\rho T_{\pi N}(k_0, k_0)] K_{\gamma\pi}(k_0, q). \quad (4.31)$$

For investigating the hadron structure, we are interested in the  $\gamma N \leftrightarrow \Delta$  vertex. As seen in Eqs. (4.24) and (4.30), the dressed vertices in the  $t$  matrix and in the  $K$  matrix are different. In the  $t$ -matrix formulation  $\bar{\Gamma}_{\gamma N, \Delta}$ , Eq. (4.24), is a complex quantity, while in the  $K$ -matrix formulation  $\bar{\Gamma}_{\gamma N, \Delta}^k$ , Eq. (4.30), is a real function. Consequently, we need to be careful about the meaning of the  $E2/M1$  ratio of the dressed  $\gamma N \leftrightarrow \Delta$  vertex. The clearest definition seems to be in

the  $K$  matrix formulation because as the energy approaches the resonance position  $M_R = m_\Delta + \Sigma_\Delta^k(M_R)$ , Eq. (4.28) is reduced to

$$K_{\gamma\pi}(E) = \frac{A}{E - M_R} + B, \quad (4.32)$$

with

$$A = \bar{\Gamma}_{\Delta \rightarrow \pi N}^k(E) \bar{\Gamma}_{\gamma N \rightarrow \Delta}^k(E), \quad (4.33)$$

$$B = k_{\gamma\pi}(E). \quad (4.34)$$

The separable form of the residue  $A$  of the  $K$  matrix leads to an interesting result that the ratio between the  $E1$  and  $M1$  multipole amplitudes of the dressed  $\gamma N \Delta$  vertex can be directly calculated from the residues of the corresponding multipole amplitudes of the  $\gamma N \rightarrow \pi N$  reaction. The reason is that both amplitudes have the same strong interaction dressed vertex in the  $P_{33}$  channel, and hence the ratio between the residues does not depend on it. Explicitly, we have

$$\begin{aligned} R_{EM} &= \left[ \frac{A(E_{1+})}{A(M_{1+})} \right]_{\gamma N \rightarrow \pi N} \\ &= \frac{\bar{\Gamma}_{\Delta \rightarrow \pi N}^k(P_{33}) \bar{\Gamma}_{\gamma N \rightarrow \Delta}^k(E_{1+})}{\bar{\Gamma}_{\Delta \rightarrow \pi N}^k(P_{33}) \bar{\Gamma}_{\gamma N \rightarrow \Delta}^k(M_{1+})} \\ &= \frac{\bar{\Gamma}_{\gamma N \rightarrow \Delta}^k(E_{1+})}{\bar{\Gamma}_{\gamma N \rightarrow \Delta}^k(M_{1+})}. \end{aligned} \quad (4.35)$$

The above relation is the basis of the model-independent analysis of Ref. [6]. We will discuss this issue in the next section.

## V. RESULTS AND DISCUSSIONS

Our first task is to determine the parameters of the effective  $\pi N$  Hamiltonian derived in Sec. II. Apart from the known  $\pi NN$  coupling constant  $f_{\pi NN}^2/4\pi = 0.08$ , the model has seven parameters: the coupling constants ( $g_\rho^2 = g_{\rho NN} g_{\rho \pi \pi}$ ,  $\kappa_\rho$ ,  $f_{\pi N \Delta}$ ) of Eqs. (3.12)–(3.16), the cutoff parameters ( $\Lambda_{\pi NN}$ ,  $\Lambda_{\pi N \Delta}$ ,  $\Lambda_\rho$ ) of the form factors (3.34)–

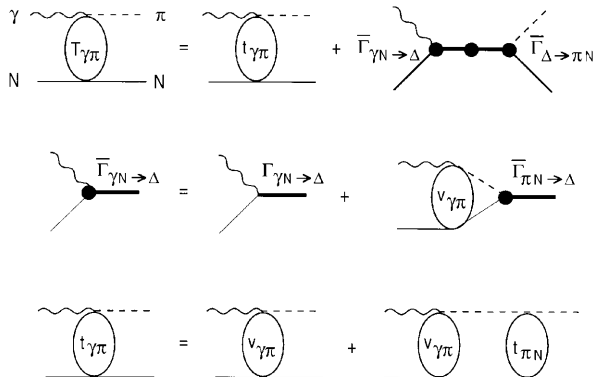


FIG. 6. Graphical representation of pion production amplitudes defined by Eqs. (4.22)–(4.24).

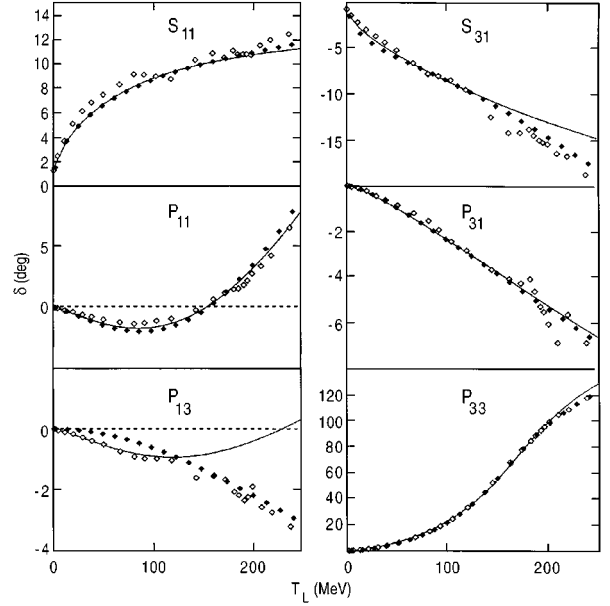


FIG. 7. The  $\pi N$  phase shifts calculated from the  $\pi N$  model L of Table I are compared with the empirical values of the analyses of Ref. [39] (open squares) and Ref. [38] (solid squares).  $T_L$  is the pion laboratory energy.

(3.37), and  $m_\Delta$  of the  $\Delta$  bare mass. These parameters are determined by fitting the  $\pi N$  phase shifts. Without including inelastic channels, our scattering equations Eqs. (3.23)–(3.30) are valid rigorously only in the energy region where the  $\pi N$  scattering is purely elastic. We therefore first take a conservative approach to only fit the data in the energy region below  $T_L = 250$  MeV pion laboratory energy. This model, called model L, is sufficient for investigating pion photoproduction up to 400 MeV photon laboratory energy. Our results are displayed in Fig. 7. We see that within the uncertainties of the phase shift data [38–40] the model can give a good account of all  $s$  and  $p$  partial waves except the  $P_{13}$  channel at  $T_L > 120$  MeV. We have found that this difficulty cannot be removed by trying various form factors other than those given in Eqs. (3.34)–(3.37), and following the previous works [12,13] to include the exchange of a fictitious scalar  $\sigma$  meson. To see the origin of this problem, we show in Fig. 8 the contributions from each mechanism of Fig. 3 to the on-shell matrix elements of the  $\pi N$  potential. Clearly, the fit to the phase shift data involves delicate cancellations between different mechanisms. It is possible to improve the fit to  $P_{13}$  by weakening the  $\rho$  exchange or the  $\Delta$  exchange. But this change will destroy the good fits to all other partial waves. Fortunately, the  $\pi N$  scattering effect due to the  $P_{13}$  channel is weak in determining the pion photoproduction cross sections. We therefore will not pursue the solution of this problem here. Perhaps this can be solved only when the  $\rho$  exchange is replaced by the two-pion exchange considered in Ref. [14]. To be consistent, the coupling with two-pion channels, such as  $\pi\Delta$  and  $\rho N$ , must also be included. These two possible improvements can be achieved by extending the unitary transformation method introduced in Secs. II–IV to second order in the coupling constants.

Let us now examine in more detail the  $P_{33}$  channel which is most relevant to our later investigation of the  $\Delta$  excitation

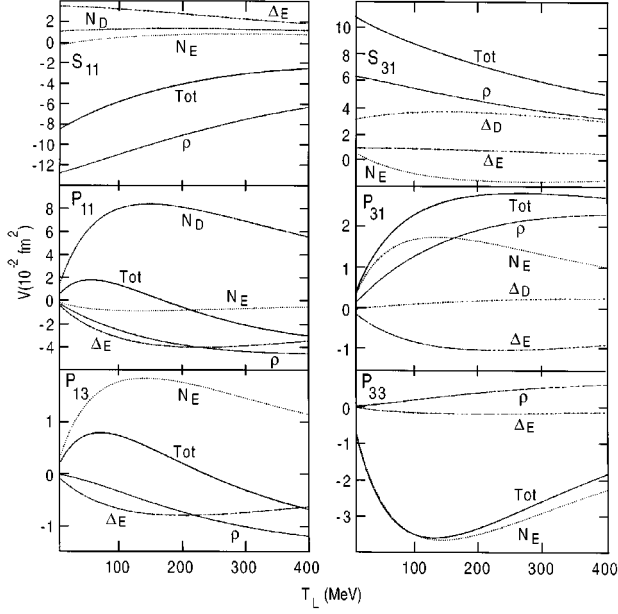


FIG. 8. The on-shell matrix elements of  $\pi N$  potentials defined by Eqs. (3.11)–(3.16).  $T_L$  is the pion laboratory energy. The notations are  $N_D : v_{N_D}$ ,  $N_E : v_{N_E}$ ,  $\rho : v_\rho$ ,  $\Delta_D : v_{\Delta_D}$ ,  $\Delta_E : v_{\Delta_E}$ , and Tot is the sum.

in pion photoproduction. As seen in Eq. (3.23), the resonant part of the  $P_{33}$  amplitude is determined by the dressed propagator  $G_\Delta$  of Eq. (3.26) and the dressed vertex  $\bar{\Gamma}_{\Delta \leftrightarrow \pi N}$  of Eqs. (3.28) and (3.29). Clearly, the  $\Delta$  resonance peak of  $\pi N$  scattering can be obtained only when the model can generate a  $\Delta$  self-energy such that the real part of  $[E - m_\Delta - \Sigma_\Delta(E)] \rightarrow 0$  as the  $\pi N$ -invariant mass  $W$  approaches the resonance energy  $W = M_R = 1236$  MeV. Our model has this desired property, as illustrated in the upper half of Fig. 9. Another important feature in the  $P_{33}$  channel is that the  $\pi N$  potential generates the dressed  $\Delta \leftrightarrow \pi N$  vertex, as defined in Eqs. (3.28) and (3.29). We have found that this renormalization effect modifies greatly the  $\Delta \leftrightarrow \pi N$  form factor in the low-momentum region. To see this, we cast the bare vertex [Eq. (3.22) including the form factor  $F_{\pi N \Delta}(k)$  defined by Eq. (3.36)] and the dressed vertex [Eq. (3.28)] into the forms

$$\langle \Delta | \Gamma_{\Delta \leftrightarrow \pi N} | \vec{k} i \rangle = -\frac{f_{\pi N \Delta}}{m_\pi} \frac{i}{\sqrt{(2\pi)^3} \sqrt{2m_\pi}} F_{\text{bare}}(k) \vec{S} \cdot \vec{k} T_i, \quad (5.1)$$

$$\langle \Delta | \bar{\Gamma}_{\Delta \leftrightarrow \pi N} | \vec{k} i \rangle = -\frac{\bar{f}_{\pi N \Delta}}{m_\pi} \frac{i}{\sqrt{(2\pi)^3} \sqrt{2m_\pi}} F_{\text{dressed}}(k) \vec{S} \cdot \vec{k} T_i, \quad (5.2)$$

with the normalization  $|F_{\text{dressed}}(0)| = F_{\text{bare}}(0) = 1$ . We find that the dressed coupling constant  $\bar{f}_{\pi N \Delta}$  is 1.3 of the bare coupling constant  $f_{\pi N \Delta}$ . The dressed form factor  $\bar{F}_{\pi N \Delta}(k)$  falls off faster than the bare form factor  $F_{\pi N \Delta}(k)$  in momentum space, as seen in the lower half of Fig. 9. This means that the nonresonant  $\pi N$  interaction has extended the  $\Delta$  excitation region to a larger distance in coordinate space.

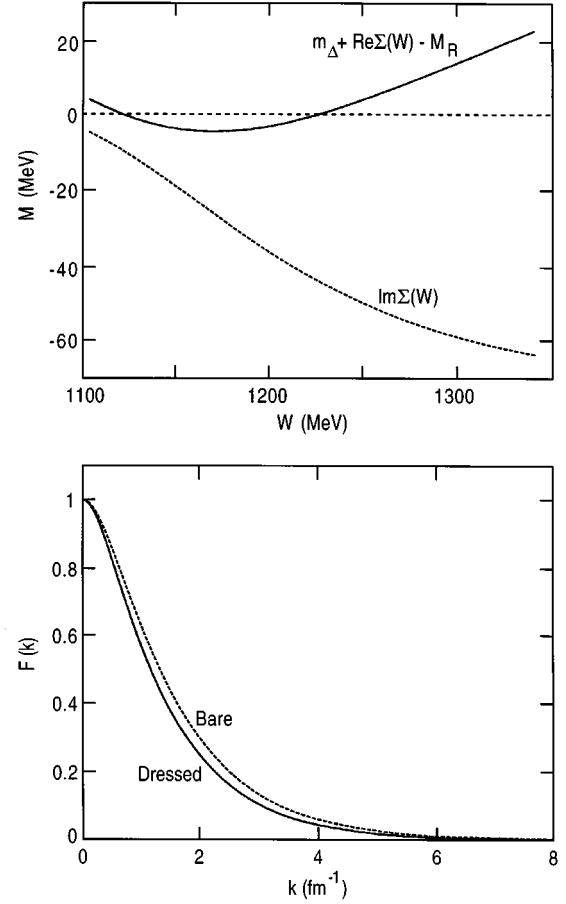


FIG. 9. The upper half shows the mass of the  $\Delta$  state defined by Eq. (3.30).  $m_\Delta = 1299.07$  MeV is the bare mass of model L of Table I,  $M_R = 1236$  is the experimental resonance position, and  $W$  is the  $\pi N$ -invariant mass. The lower half shows the bare and dressed  $\Delta \leftrightarrow \pi N$  form factors defined by Eqs. (5.1) and (5.2) with  $\bar{f}_{\pi N \Delta} = 1.3 f_{\pi N \Delta}$ .  $k$  is the pion momentum in the  $\Delta$  rest frame.

A significant difference between our approach and the previous  $\pi N$  models [12–14,19] is in the treatment of the  $P_{11}$  channel. By employing the unitary transformation, the  $\pi N \leftrightarrow N$  vertex does not appear in the effective Hamiltonian, Eq. (3.8), and hence our formulation of  $\pi N$  scattering is straightforward. It does not require the nucleon mass renormalization. It is natural to ask whether our approach possesses the well-established nucleon-pole dynamics. This question can be answered by examining Fig. 10 in which the  $\pi N$  phase shifts and the scattering  $t$ -matrix elements calculated from the nucleon pole term  $v_{N_D}$  only [Fig. 3(c)] and the full potential are compared. We see in the upper half of Fig. 10 that  $\pi N$  phase shifts due to the nucleon-pole term (dotted curve) are repulsive as expected. The fit to the  $P_{11}$  data is due to a delicate cancellation between the repulsive nucleon-pole term and the attraction coming mainly from  $\rho$ - and  $\Delta$ -exchange terms (see the  $P_{11}$  case in Fig. 8). In the lower half of Fig. 10, we see that as the energy approaches the threshold,  $W = m_\pi + m_N$ , the nucleon pole term (dotted curve) apparently dominates the interaction. If we analytically continue to the nucleon pole position,  $k_0 = ik_N$  [ $m_N = E_N(ik_N) + E_\pi(ik_N)$ ], the scattering amplitude will be determined by the nucleon pole term, i.e.,

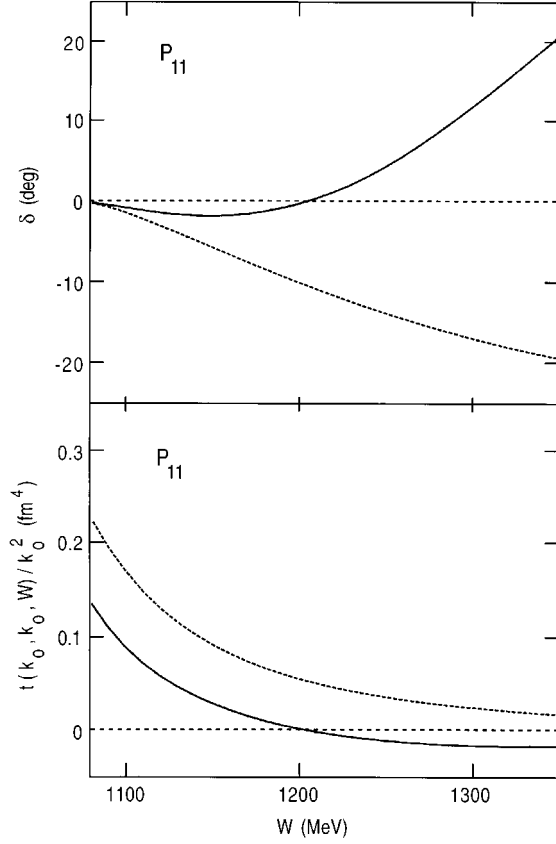


FIG. 10. The  $\pi N$  phase shifts ( $\delta$ ) and scattering amplitude [ $t(k_0, k_0, W)$ ] with the  $\pi N$ -invariant mass  $W = E_N(k_0) + E_\pi(k_0)$  in the  $P_{11}$  channel. The solid curves are from the full calculation. The dotted curves are from the calculation including only the nucleon pole potential  $v_{N_D}$  of Fig. 3(c).

$$t(k_0, k_0, W \rightarrow m_N) \sim v_{N_D} \sim 1/(W - m_N).$$

The parameters of the constructed model are listed in the first row (model L) of Table I. The calculated scattering lengths are presented in the first column of Table II. They are all in good agreement with the data. If we assume the universality of  $\rho$  coupling, we then have  $g_{\rho NN} = g_{\rho\pi\pi} = 6.2$  which is close to that determined in Refs. [12,13]. The fit is also sensitive to the  $\rho$  tensor coupling constant  $\kappa_\rho$ . Our value is close to that of Ref. [12], but is much smaller than 6.6 used in Ref. [13].

We now turn to presenting our results of pion photoproduction. With the  $\pi NN$ ,  $\pi\Delta N$ , and  $\rho NN$  vertices defined by the parameters given in Table I, the considered pion photo-

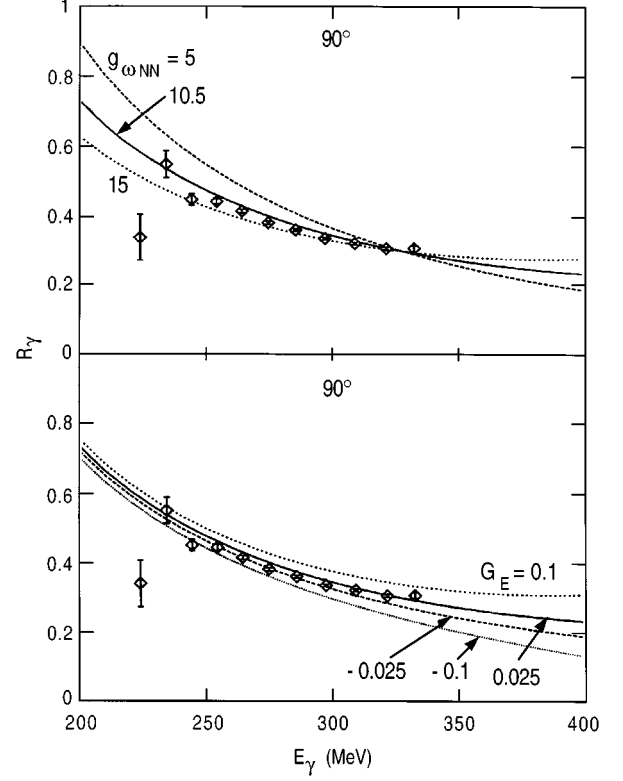


FIG. 11. The photon-asymmetry ratios  $R_\gamma = d\sigma_{\parallel}/d\sigma_{\perp}$  of  $\gamma p \rightarrow \pi^0 p$  at  $90^\circ$ .  $E_\gamma$  is the photon energy in the laboratory frame. The results in the upper half are from using  $G_M = 1.85$ ,  $G_E = 0.025$ , and three values of  $g_{\omega NN}$ . The results in the lower half are from using  $G_M = 1.85$ ,  $g_{\omega NN} = 10.5$ , and four values of  $G_E$ . The data are from Refs. [41,42].

production mechanisms (Fig. 5) still have unknown parameters associated with the vector meson-exchange and the  $\gamma N \leftrightarrow \Delta$  vertex. Following the previous approach [17], we assume that the photon-meson coupling constants  $g_{\rho\pi\gamma}$  and  $g_{\omega\pi\gamma}$  can be determined from the partial decay widths listed by the Particle Data Group [45]. For the  $\omega$  meson, we further assume that the tensor coupling  $\kappa_{\omega NN} = 0$  and the  $\omega NN$  form factor is identical to the  $\rho NN$  form factor given in Table I. The coupling constant  $g_{\omega NN}$  is not well determined in the literature. We will treat it as a free parameter, although the quark model value  $g_{\omega NN} = (3g_{\rho NN})/2$  seems to be a reasonable guess. Thus, our investigation of pion photoproduction has only three adjustable parameters:  $G_M$  and  $G_E$  of the bare  $\Delta \leftrightarrow \gamma N$  vertex, and the coupling constant  $g_{\omega NN}$  of the  $\omega$

TABLE I. The parameters of the  $\pi N$  models. The units are 1/F for cutoff parameters  $\Lambda_\alpha$  and MeV for the bare  $\Delta$  mass. Model L and model H are obtained respectively from fitting  $\pi N$  phase shifts up to 250 MeV and 400 MeV.

Model	$f_{\pi NN}^2/4\pi$	$\Lambda_{\pi NN}$	$g_{\rho NN}g_{\rho\pi\pi}$	$\kappa_\rho$	$\Lambda_\rho$	$f_{\pi N\Delta}$	$\Lambda_{\pi N\Delta}$	$m_\Delta$
Model L	0.08	3.2551	38.4329	1.825	6.2305	2.049	3.29	1299.07
Model H	0.08	3.7447	39.0499	2.2176	7.5569	2.115	3.381	1318.52

$$\text{Form factor } F_{\pi NN}(k) = \left( \frac{\Lambda_{\pi NN}^2}{\Lambda_{\pi NN}^2 + k^2} \right)^2, \quad F_\rho(q) = \left( \frac{\Lambda_\rho^2}{\Lambda_\rho^2 + q^2} \right)^2, \quad F_{\pi N\Delta}(k) = \left( \frac{\Lambda_{\pi N\Delta}^2}{\Lambda_{\pi N\Delta}^2 + k^2} \right)^2$$

TABLE II. The calculated  $\pi N$  scattering lengths (in unit of fermis) are compared with the values determined in Ref. [40].

	Model L	Model H	Koch-Pietarinen
$S_{11}$	0.1588	0.1737	$0.173 \pm 0.003$
$S_{31}$	-0.1191	-0.1198	$-0.101 \pm 0.004$
$P_{11}$	-0.0976	-0.0864	$-0.081 \pm 0.002$
$P_{31}$	-0.0509	-0.0478	$-0.045 \pm 0.002$
$P_{13}$	-0.0363	-0.0383	$-0.030 \pm 0.002$
$P_{33}$	0.2523	0.2797	$0.214 \pm 0.002$

exchange. We have, however, some ideas about the ranges of these parameters. If we assume that bare vertex interaction  $\Gamma_{\Delta \rightarrow \gamma N}$  can be identified with the constituent quark model [46,48,47,49,50], then  $|G_E/G_M| \sim 0$  since the one-gluon exchange interaction gives negligible  $D$ -state components in  $N$  and  $\Delta$ . We also expect that the  $\omega$  coupling should be close to the quark model prediction,  $g_{\omega NN} = 3g_{\rho NN}/2 \sim 9$ , if the  $\rho$  coupling from our  $\pi N$  model (Table I) is used. It is therefore reasonable to only consider the region  $g_{\omega NN} \leq 15$  and  $|G_E/G_M| \leq 0.1$ .

Since the  $\omega$ -exchange mechanism [Fig. 5(g)] does not produce charged pions directly (only through  $\pi N$  charge exchange), the ranges of  $g_{\omega NN}$ ,  $G_M$ , and  $G_E$  can be most sensitively determined by considering the data of  $\pi^0$  photo-production. In the considered region that  $|G_E/G_M| \leq 0.1$  and  $g_{\omega NN} \leq 15$ , we have found that the magnitudes of the  $\pi^0$  differential cross sections depend mainly on  $G_M$ . The values of  $g_{\omega NN}$  and  $G_E$  can be narrowed down by considering spin observables. In this work, we make use of the recent LEGS [41] data of photon-asymmetry ratios  $R_\gamma = d\sigma_{\parallel}/d\sigma_{\perp}$  of  $\gamma p \rightarrow \pi^0 p$  reaction. We have found that the slope of  $R_\gamma(E)$  at a fixed pion angle is sensitive to the value of  $g_{\omega NN}$ . This is illustrated in the upper half of Fig. 11 for the case of  $G_M = 1.85$  and  $G_E = 0.025$ . A smaller  $g_{\omega NN}$  yields a steeper slope. The data clearly favor  $g_{\omega NN} \sim 10.5$ . In the lower half of Fig. 11, we see that the magnitude, not the slope, of  $R_\gamma$  is significantly changed by varying the value of  $G_E$  from  $-0.1$  to  $+0.1$ . The data are consistent with  $-0.025 \leq G_E \leq 0.025$ , while  $G_E = +0.025$  seems to give a better fit. Results similar to Fig. 11 can be obtained by using a higher value  $G_M = 1.95$ . In this case, a smaller value of  $g_{\omega NN} = 7$  is needed to maintain the same fit to the magnitude of the differential cross section as well as the slope of the  $R_\gamma$ . But the best value of  $G_E$  to reproduce the magnitude of  $R_\gamma$  is  $-0.025$  instead of  $+0.025$  for the  $g_{\omega NN} = 10.5$  case. In fact, we have observed a strong correlation between the allowed values of  $G_M$  and  $g_{\omega NN}$ . In all cases, the allowed value of  $G_E$  is consistent with  $-0.025 \leq G_E \leq +0.025$ . Therefore, the acceptable values of  $(G_M, g_{\omega NN})$  are on the curve between the  $G_E = -0.025$  and  $G_E = +0.025$  lines in Fig. 12. To determine the precise value of  $R_{EM} = G_E/G_M$ , which measures the deformation of the  $\Delta$ , we clearly need to pin down the  $\omega$  meson coupling constant  $g_{\omega NN}$ . In Table III, we list the determined values of  $G_M$ ,  $G_E$ , and  $g_{\omega NN}$  along with all other parameters used in our calculations of  $\gamma N \rightarrow \pi N$  reactions.

The predictions from using the parameters lying on the curve between  $G_E = +0.025$  and  $G_E = -0.025$  lines of Fig.

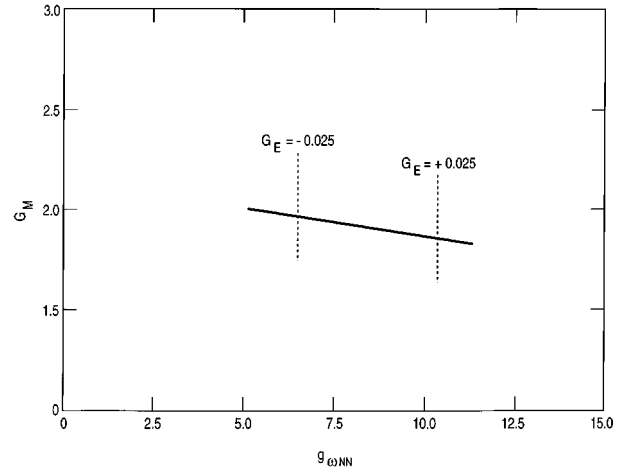


FIG. 12. The region of the parameters  $(g_{\omega NN}, G_M, G_E)$  for describing the data of  $\gamma N \rightarrow \pi N$  reactions. See text for the explanations.

12 are also in good agreement with the  $\pi^0$  data at other angles and the  $\pi^+$  data. These are shown in Fig. 13 for  $\pi^0$  production and Fig. 14 for  $\pi^+$  production. These results are obtained from using the parameters defined by the interaction points of the  $G_E = \pm 0.025$  lines in Fig. 12:  $(g_{\omega NN}, G_M, G_E) = (10.5, 1.85, +0.025)$ , and  $(7.0, 1.95, -0.025)$ . Both sets of parameters yield equally good agreement with the  $\pi^0$  data (Fig. 13). For  $\pi^+$  production, the predictions are in good agreements with the data of the photon-asymmetry ratios  $R_\gamma$ , but underestimate the differential cross sections by about 10% at most energies. Since the  $\omega$  exchange has a small contribution to the  $\pi^+$  production (only through charge-exchange  $\pi N$  final state interaction), the only way to resolve this difficulty within our model is to increase the value of  $G_M$ . But this will lead to an overestimate of the  $\pi^0$  cross section from Bonn.

Although the difficulty in reproducing the  $\pi^+$  data in Fig. 14(b) could be an indication of the deficiency of our model, the possibility of a larger  $\pi^0$  cross section has been suggested by three  $\pi^0$  data at  $\theta = 120^\circ$  from Ref. [44] [Fig. 13(b)]. To fit these three data points, we need to increase  $G_M$  from 1.85 to 2.0 for the case of  $g_{\omega NN} = 10.5$  and from 1.95 to 2.1 for the case of  $g_{\omega NN} = 7$ . The results from these two changes in  $G_M$  are, respectively, the solid and dotted

TABLE III. The parameters for the  $\gamma N \rightarrow \pi N$  interactions defined in Eqs. (4.16)–(4.20) and Fig. 5.

$f_{\pi NN}, \Lambda_{\pi NN}$	–	Table I
$f_{\pi N\Delta}, \Lambda_{\pi N\Delta}$	–	Table I
$g_{\rho NN} = \sqrt{g_{\rho NN} g_{\rho\pi\pi}}$	–	Table I
$\Lambda_{\rho NN} = \Lambda_\rho, \kappa_\rho$	–	Table I
$g_{\rho\pi\gamma}$	$0.1027e$	Ref. [45]
$g_{\omega\pi\gamma}$	$0.3247e$	Ref. [45]
$g_{\omega NN}$	$7 - 10.5$	See text
$\Lambda_{\omega NN} = \Lambda_\rho$	–	Table I
$\kappa_\omega = 0$	–	See text
$G_M(0)$	$1.85 - 2.0$	See text
$G_E(0)$	$\pm 0.025$	See text

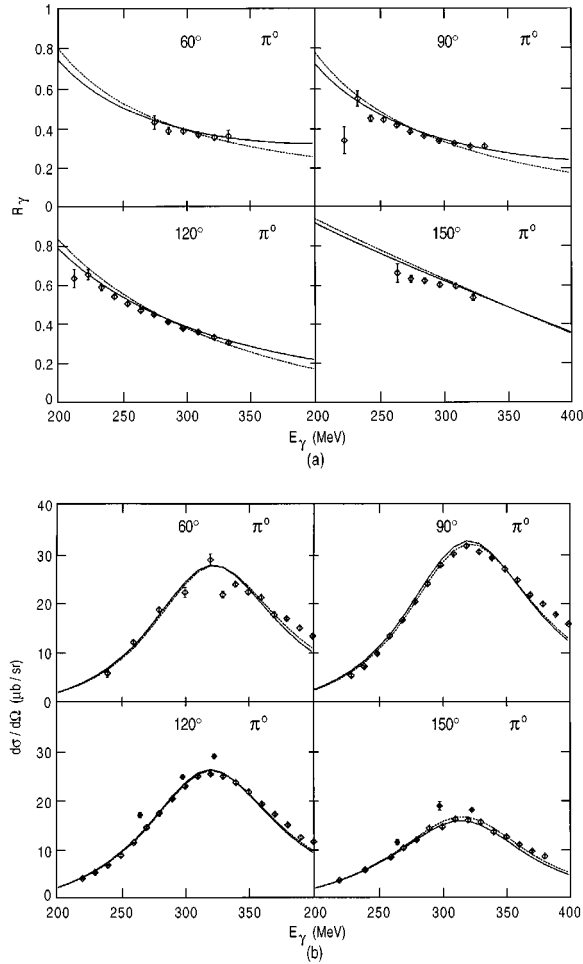


FIG. 13. The photon-asymmetry ratios (a) and differential cross sections (b) for the  $\gamma p \rightarrow \pi^0 p$  reaction at four angles in the center-of-mass frame. The solid and dotted curves are, respectively, from the calculation using the parameters  $(g_{\omega NN}, G_M, G_E) = (10.5, 1.85, +0.025)$ , and  $(7.0, 1.95, -0.025)$ . The data are from Refs. [41,42].  $E_\gamma$  is the photon energy in the laboratory frame.

curves in Figs. 15 and 16. The predicted photon-asymmetry ratios [Figs. 15(a) and 16(a)] are still in good agreement with the data. The agreement with the  $\pi^+$  data [Fig. 16(b)] is clearly improved. But the calculated  $\pi^0$  differential cross sections [Fig. 15(b)] overestimate the Bonn data [42,43] by about 15%. Clearly, the disagreement between the  $\pi^0$  data at  $\theta = 120^\circ$  [Fig. 15(b)] from Refs. [42,43] and [44] must be resolved by new measurements.

To further reveal the dynamical content of our model, we compare in Fig. 17 our predictions of angular distributions with the data compiled in Ref. [43] for  $\gamma p \rightarrow \pi^0 p$  [Fig. 17(a)],  $\gamma p \rightarrow \pi^+ n$  [Fig. 17(b)], and  $\gamma n \rightarrow \pi^- p$  [Fig. 17(c)] reactions. All results calculated from using the parameters lying on the curve between the  $G_E = +0.025$  and  $G_E = -0.025$  lines in Fig. 12 are very close to the solid curves which are from using  $(g_{\omega NN}, G_M, G_E) = (10.5, 1.85, 0.025)$ . Again, we see that the charged pion production cross sections are underestimated. If a larger  $G_M = 2.0$  is used in this calculation, we obtain the dotted curves which are in a better agreement with the charged pion data, but overestimate the  $\pi^0$  data by about 15% at reso-

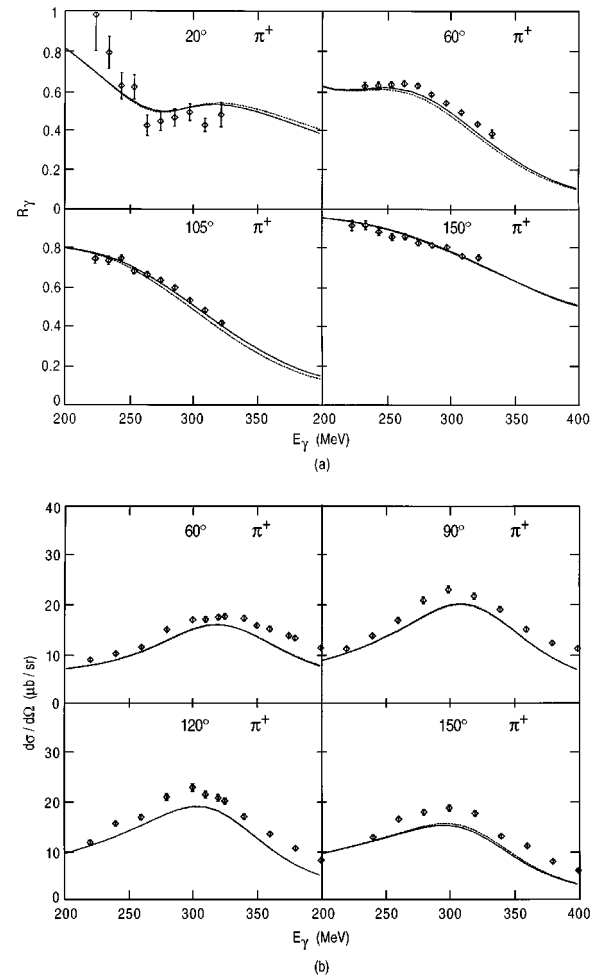


FIG. 14. Same as Fig. 13, except for the  $\gamma p \rightarrow \pi^+ n$  reaction. The data are from Ref. [42].

nance peaks. In all cases, the theoretical predictions underestimate the data at 380 MeV and higher energies. This is expected, since the constructed model does not include inelastic channels which should start to play a significant role at energies above about 350 MeV. For example, the inelastic production mechanism  $\gamma N \rightarrow \pi \Delta \rightarrow \pi N$  should exist since it is known that the  $\pi N$  scattering at this higher energy can be described only when the coupling with the  $\pi \Delta$  channel is included. To investigate this effect, it is necessary to extend the derivation of effective Hamiltonians presented in Secs. III and IV to include the  $\pi \Delta$  as well as other two-pion states.

We now focus on the theoretical interpretations of the  $\Delta \leftrightarrow \gamma N$  vertex. The values of  $G_M$  and  $G_E$  determined above characterize the bare  $\Delta \leftrightarrow \gamma N$  vertex which can only be identified with hadron models with no coupling with the  $\pi N$  or other hadronic reaction channels. One possible interpretation is to compare the determined  $G_M$  and  $G_E$  with the predictions of the most well-developed constituent quark model [46,48,47,49,50]. To explore this possibility, it is necessary to first discuss the quantities in our model which can be compared with the results from empirical amplitude analyses [6,7,57]. For investigating the  $\Delta$  mechanism, we need to only consider the  $\gamma N \rightarrow \pi N$  multipole amplitudes  $M_{1+}$  and  $E_{1+}$  with a  $P_{33}$  final  $\pi N$  state and the dressed vertex func-



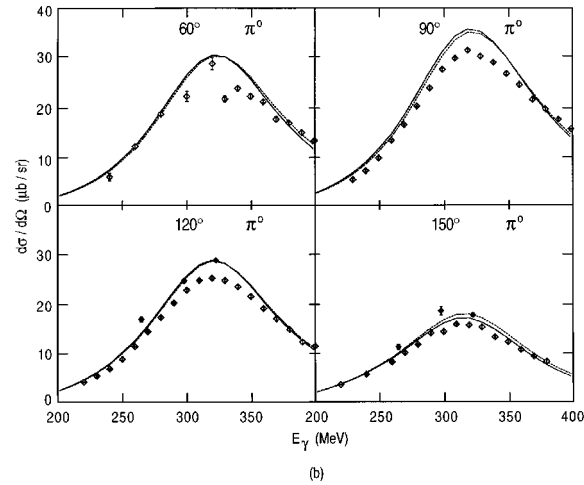
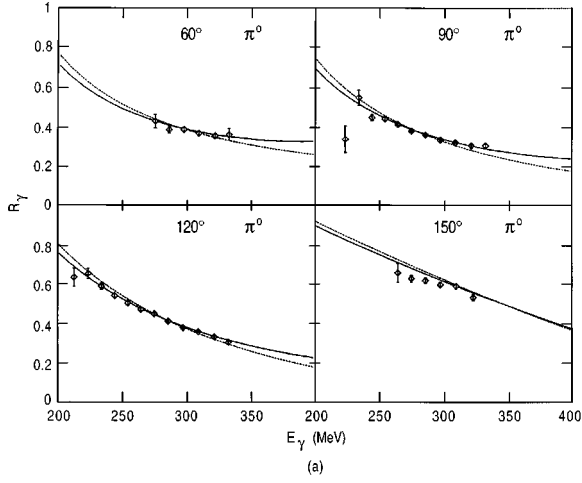


FIG. 15. The photon-asymmetry ratios (a) and differential cross sections (b) for the  $\gamma p \rightarrow \pi^0 p$  reaction at four angles. The solid and dotted curves are, respectively, from the calculations using the parameters  $(g_{\omega NN}, G_M, G_E) = (10.5, 2.0, +0.025)$ , and  $(7.0, 2.10, -0.025)$ . The data are from Refs. [41,42].  $E_\gamma$  is the photon energy in the laboratory frame.

tion  $\bar{\Gamma}_{\gamma N, \Delta}$ . These can be computed from Eqs. (4.22)–(4.24) or Eqs. (4.28)–(4.30) by performing the standard partial-wave decomposition (see, for example, the Appendix of Ref. [17]). We will discuss these quantities using the results calculated from setting  $(g_{\omega NN}, G_M, G_E) = (10.5, 1.85, 0.025)$  (solid curves in Figs. 13, 14, and 17).

The predicted amplitudes  $M_{1+}$  and  $E_{1+}$  are compared in Fig. 18 with the results from the empirical amplitude analyses [7,57]. We see in the upper part of Fig. 18 that the predicted  $M_{1+}$  amplitudes are in good agreement with empirical values. In the lower half, we show that both the  $E_{1+}$  amplitudes calculated from using  $G_E = +0.025$  (solid curves) and  $G_E = -0.025$  (dotted curves) are within the uncertainties of the amplitude analyses. This is consistent with our analysis using LEGS data, as seen in the lower part of Fig. 11. The uncertainties of the empirical values of the  $E_{1+}$  amplitude are due to the lack of complete data of spin observables. More experimental efforts are clearly needed to pin down the value of  $G_E$  which is needed to test models of hadron structure.

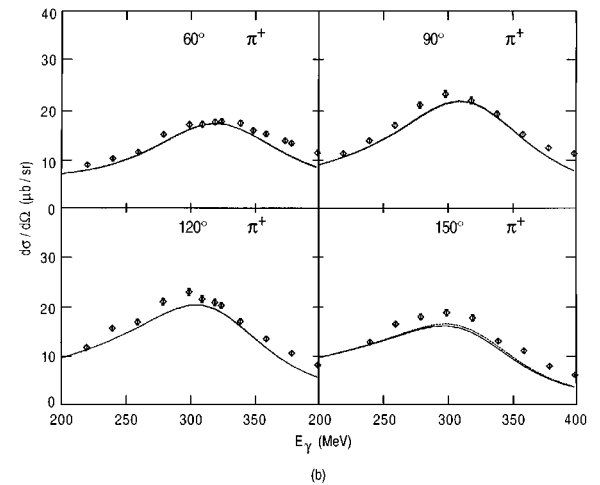
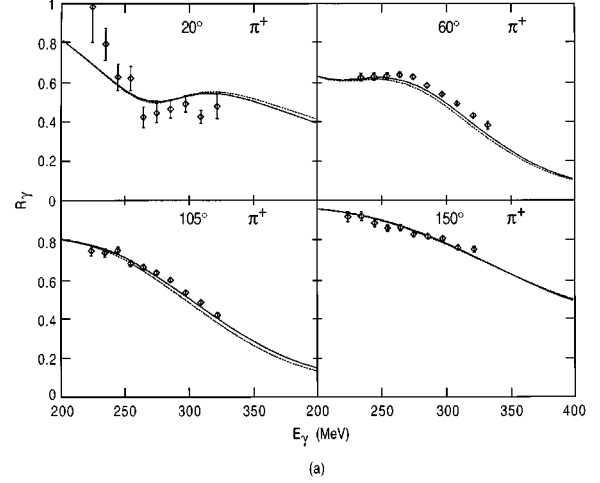


FIG. 16. Same as Fig. 15, except for the  $\gamma p \rightarrow \pi^+ n$  reaction. The data are from Ref. [42].

The dressed  $\Delta \leftrightarrow \gamma N$  vertex, defined by Eq. (4.24), is a complex number. By making the usual partial-wave decomposition, its magnetic  $M1$  and electric  $E2$  components can be written as  $\Gamma(\alpha) = |\Gamma(\alpha)| e^{i\phi(\alpha)}$  with  $\alpha = M_{1+}, E_{1+}$ . The predicted dressed vertex functions  $\Gamma(\alpha)$  are the solid curves in Fig. 19. We see that their magnitudes  $|\Gamma(\alpha)|$  are very different from the corresponding values (dotted curves) of the bare  $\Delta \leftrightarrow \gamma N$  vertex. The differences are due to the very large contribution of the nonresonant mechanism described by the second term of Eq. (4.24). Our results indicate that an accurate reaction theory calculation of the nonresonant pion photoproduction mechanisms is needed to determine the bare  $\Delta \leftrightarrow \gamma N$  vertex from the pion photoproduction data. This requires a dynamical treatment of the nonresonant pion photoproduction mechanisms, as we have done in this work. Within the meson-exchange formulation presented in this work, the determined  $G_M$  and  $G_E$  of the bare  $\Delta \leftrightarrow \gamma N$  vertex can be compared with the predictions from a hadron model which does not include the coupling with the  $\pi N$  “reaction” channel (both pion and nucleon are on their mass shell).

We now turn to investigate the  $K$ -matrix method which has been the basis of the empirical amplitude analyses of Refs. [6,7]. In Ref. [6], it was shown that if the background term is assumed to be a slowly varying function of energy,

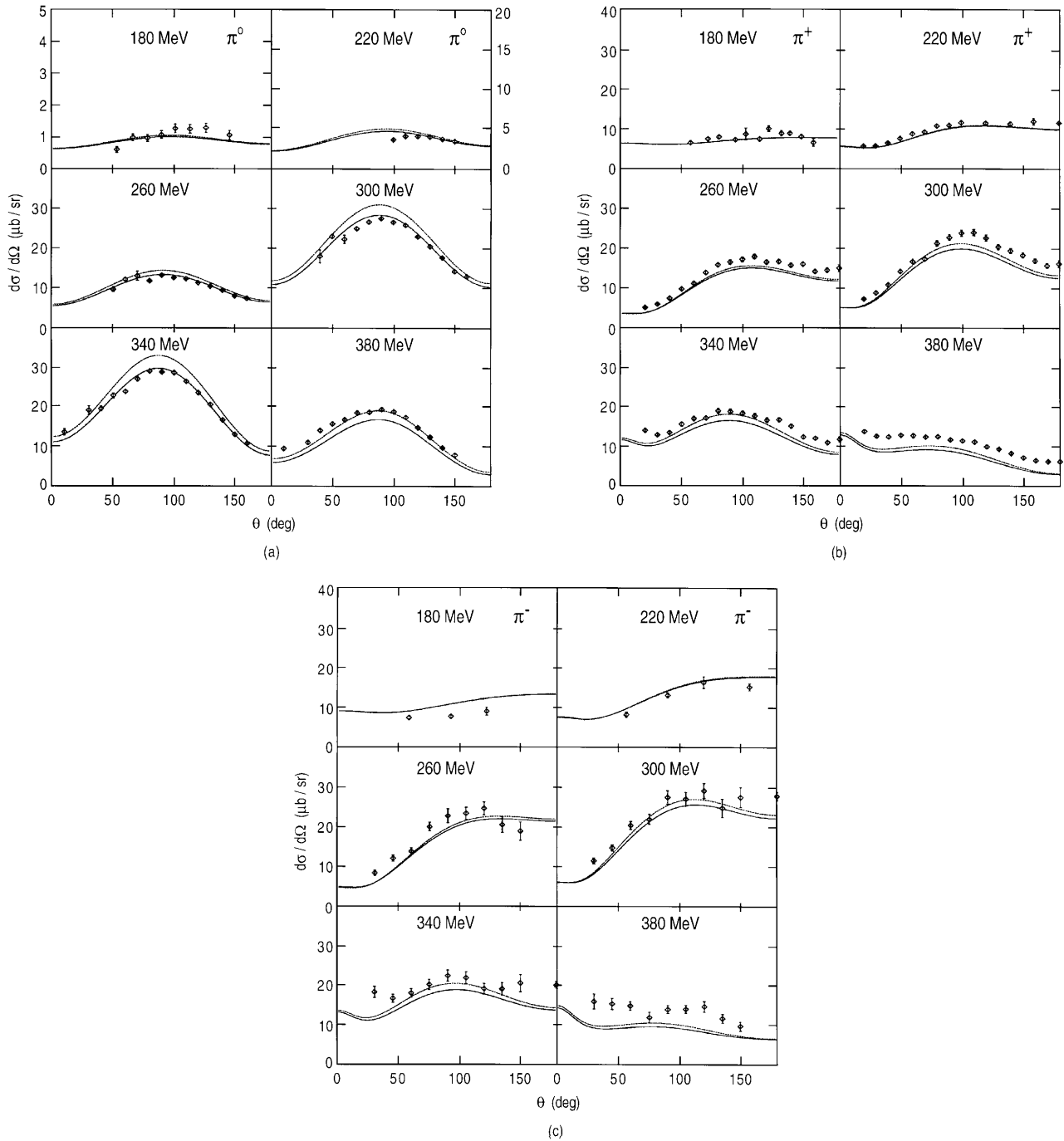


FIG. 17. Differential cross sections of  $\gamma p \rightarrow \pi^0 p$  (a),  $\gamma p \rightarrow \pi^+ n$  (b), and  $\gamma n \rightarrow \pi^- p$ , (c) reactions. The solid (dotted) curves are calculated by using  $G_M = 1.85$  (2.0). Both calculations using the same  $(g_{\omega NN}, G_E) = (10.5, +0.025)$ . The data are from Ref. [43].  $E_\gamma$  is the photon energy in the laboratory frame.

the ratio  $R_{EM}$  between the  $E_{1+}$  and  $M_{1+}$  of the  $\gamma N \rightarrow \Delta$  transition at the resonant energy  $W = M_R$  can then be extracted “model independently” from the data of the  $\gamma N \rightarrow \pi N$  reaction. The only limitation is the accuracy of the employed  $\pi N$  amplitudes and the  $M_{1+}$  and  $E_{1+}$  multipole amplitudes of the  $\gamma N \rightarrow \pi N$  reaction. By using Eqs. (4.32)–(4.35), we can examine whether the  $K$ -matrix method of Ref. [6] is consistent with our dynamical model. In Fig. 20, we display our predictions of the energy dependence of the total  $K$  matrix (solid curve), the contribution from the resonant term (dotted curve) which has a pole at  $W = 1236$  MeV, and

the nonresonant contribution  $B$  (dashed curve). Clearly, the energy dependence of the nonresonant term  $B$  is rather weak. The assumption made in the empirical analysis of Ref. [6] is fairly consistent with our dynamical model.

By using Eq. (4.33), we can calculate the residue  $A$  of the  $K$  matrix from the dressed vertex  $\bar{\Gamma}_{\gamma N \rightarrow \Delta}^k$  defined by Eq. (4.30). The results (solid curve) for the  $M_{1+}$  transitions are compared with that calculated from using the bare vertex  $\Gamma_{\gamma N \rightarrow \Delta}$  in the upper half of Fig. 21. Similar to the results in Fig. 19 in the  $t$ -matrix formulation, we see the large nonresonant mechanisms in dressing the  $\gamma N \rightarrow \Delta$  vertex. The

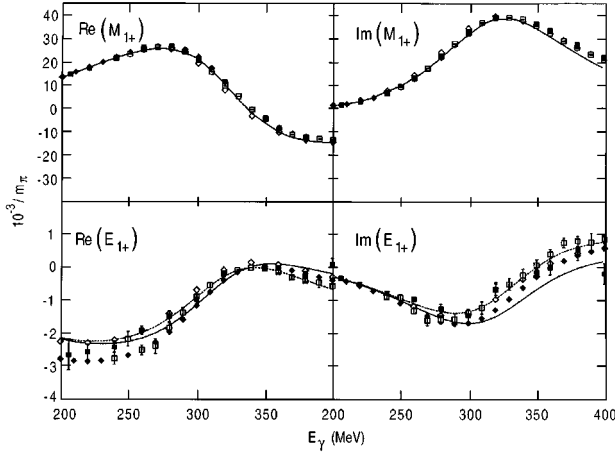


FIG. 18. The predicted multipole amplitudes  $M_{1+}$  and  $E_{1+}$  in the total isospin  $I=3/2$  channel are compared with the empirical values of Refs. [38] (solid squares) and [57] (open squares). The parameters used in this calculation are  $G_M=1.85$ ,  $g_{\omega NN}=10.5$ , with  $G_E=0.025$  (solid curve) and  $-0.025$  (dotted curve).  $E_{\gamma}$  is the photon energy in the laboratory frame.

corresponding  $E_2/M_1$  ratios  $R_{EM}$  are compared in the lower half of Fig. 21. The nonresonant mechanisms change the ratio by a factor of about 2 at resonance energy  $W=1236$  MeV.

In Table IV, we list the predicted  $E_{1+}$  and  $M_{1+}$  amplitudes of the  $\Delta \leftrightarrow \gamma N$  vertex evaluated at the resonance energy  $W=1236$  MeV. The parameters  $(g_{\omega NN}, G_M, G_E) = (10.5, 1.85, 0.025)$  and  $(7.0, 1.95, -0.025)$  from the fits to the data (Figs. 13 and 14) are used in these calculations. We see that our average value  $R_{EM} = (-1.8 \pm 0.9)\%$  is not too different from the average value  $(-1.07 \pm 0.37)\%$  of the empirical analysis [6]. Since the assumption made in Ref. [6] is consistent with our model as discussed above, the difference perhaps mainly comes from the experimental uncertainties of the multipole amplitudes employed in the analysis of

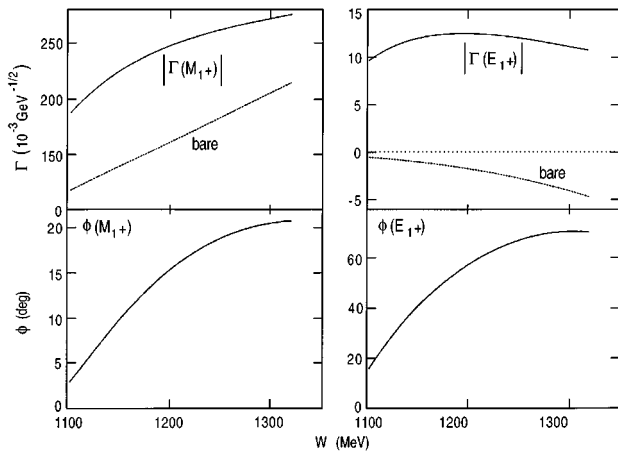


FIG. 19. The  $M_{1+}$  and  $E_{1+}$  multipole amplitudes of the dressed vertex  $\bar{\Gamma}_{\gamma N \rightarrow \Delta}$  defined by Eq. (4.24) and the bare vertex  $\Gamma_{\gamma N \rightarrow \Delta}$  are compared. The dressed vertex is a complex function written as  $\Gamma(\alpha) = |\Gamma(\alpha)|e^{i\phi(\alpha)}$  with  $\alpha = M_{1+}, E_{1+}$ .  $W$  is the  $\gamma N$ -invariant mass.

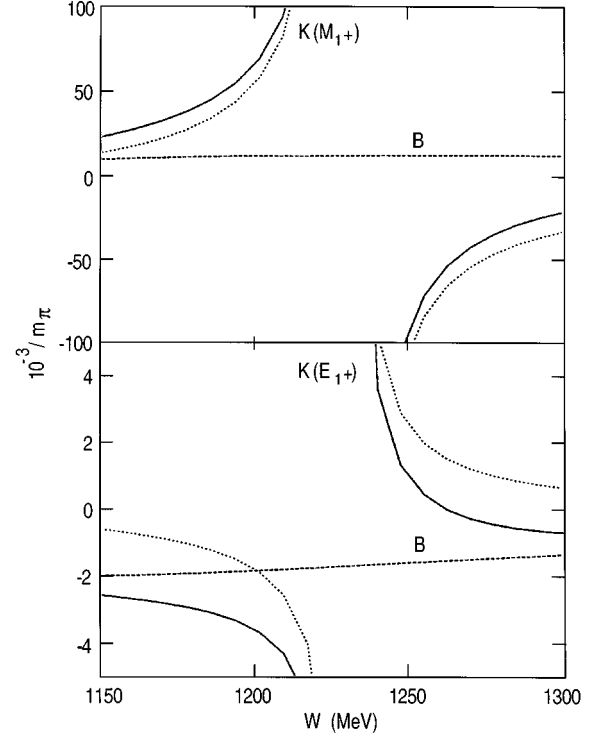


FIG. 20. The predicted  $K$  matrix defined by Eq. (4.28). The solid curves are the full calculations. The dotted curves are from the resonant term. The dashed curves (denoted as  $B$ ) are the contributions from the nonresonant term  $k_{\gamma\pi}$  defined by Eq. (4.29).  $W$  is the  $\gamma N$ -invariant mass.

Ref. [6]. The differences between our predicted multipole amplitudes and the empirical values shown in Fig. 18 could also be responsible to this discrepancy. To compare our results with the values listed by the Particle Data Group (PDG) [45], we calculate the helicity amplitudes by

$$A_{3/2} = \frac{\sqrt{3}}{2} [E_{1+} - M_{1+}],$$

$$A_{1/2} = -\frac{1}{2} [3E_{1+} + M_{1+}].$$

The results at the resonance energy  $W=1236$  MeV are listed in Table V. The predictions from two constituent quark models [48,47] are also listed for comparison. We notice that our bare values are close to the constituent quark model predictions [47,48], and the dressed values are close to the values of the PDG [45]. This suggests that our bare vertex can be identified with the constituent quark model. The long-standing discrepancy between the constituent quark model predictions and the PDG values is due to the nonresonant meson-exchange production mechanisms which must be calculated from a dynamical approach. Similar considerations must be taken in comparing the PDG values with the predictions of higher mass  $N^*$  resonances from hadron models.

The results we have presented so far are based on the  $\pi N$  model determined in a fit to the  $\pi N$  phase shifts only up to 250 MeV. It is interesting to see the extent to which this model can be extended to a higher-energy region where the inelastic processes are still not dominant. More importantly,

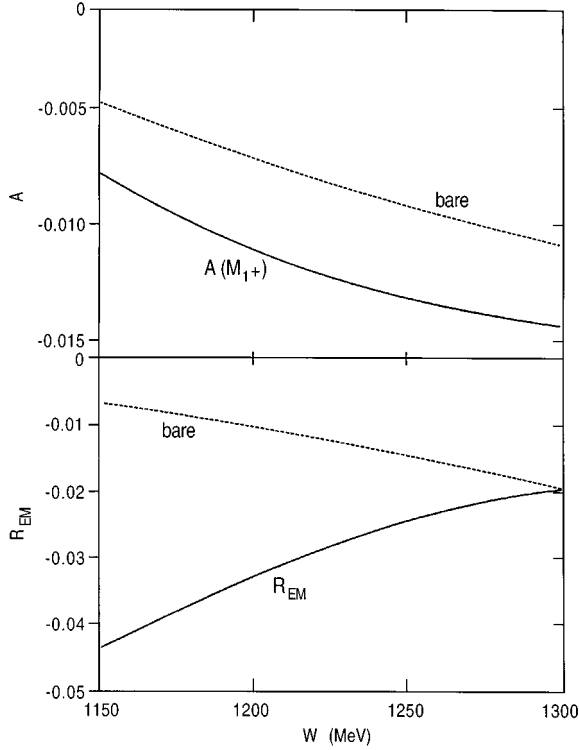


FIG. 21. The  $M_{1+}$  residues  $A$  of the  $K$  matrix [Eq. (4.32)] calculated from the dressed  $\Delta \rightarrow \gamma N$  defined by Eq. (4.30) and the bare vertex are compared in the upper half. Their corresponding ratios  $R_{EM} = E_{1+}/M_{1+}$  are compared in the lower half.  $W$  is the  $\gamma N$ -invariant mass.

we would like to examine whether the extended model can yield significantly different  $\pi N$  off-shell dynamics which perhaps can help resolve the difficulty in reproducing the magnitudes of  $\pi^+$  cross section [see Fig. 14(b)]. To explore these possibilities, a  $\pi N$  model is constructed by fitting the phase shifts data up to 400 MeV. This model is called model H to distinguish it from model L from the fit up to only 250 MeV. The resulting parameters are also listed in Table I. The phase shifts calculated from these two models are compared in Fig. 22. We see that model H (dotted curves) clearly gives a much better fit to the data in the entire considered energy region. But it is not as accurate as model L in describing the

TABLE IV. The magnetic  $M_{1+}$  and electric  $E_{1+}$  amplitudes of  $\Delta \rightarrow \gamma N$  transition at  $W = 1236$  MeV.  $R_{EM} = E_{1+}/M_{1+}$ . The amplitudes are in units of  $10^{-3} (\text{GeV})^{-1/2}$ . The numbers in the upper and lower rows for each case are respectively from using  $(g_{\omega NN}, G_M, G_E) = (10.5, 1.85, +0.025)$  and  $(7.0, 1.95, -0.025)$ .

	$M_{1+}$	$E_{1+}$	$R_{EM}$	Average
$\Gamma_{\Delta \rightarrow \gamma N}$ (bare)	175	-2.28	-1.3%	$(0.0 \pm 1.3)\%$
	184	+2.28	+1.2%	
$\bar{\Gamma}_{\Delta \rightarrow \gamma N}$ (dressed)	257	-6.9	-2.7%	$(-1.8 \pm 0.9)\%$
	258	-2.26	-0.9%	

TABLE V. Helicity amplitudes of the  $\Delta \rightarrow \gamma N$  transition at  $W = 1236$  MeV are compared with the values from Particle Data Group (PDG) [45] and the predictions of constituent quark models of Refs. [47,48]. The amplitudes are in units of  $10^{-3} (\text{GeV})^{-1/2}$ . The numbers in the upper and lower rows for each case are, respectively, from using  $(g_{\omega NN}, G_M, G_E) = (10.5, 1.85, +0.025)$  and  $(7.0, 1.95, -0.025)$ .

$A$	PDG	Dressed	Bare	Ref. [48]	Ref. [47]
$A_{3/2}$	$-257 \pm 8$	-228	-153	-157	-186
		-225	-158		
$A_{1/2}$	$-141 \pm 5$	-118	-84	-91	-108
		-126	-96		

the crucial  $P_{33}$  channel in the low-energy region. To accurately fit the  $P_{33}$  in the entire energy region and to resolve the difficulty in the  $P_{13}$  channel, additional mechanisms may be needed.

The  $\gamma N \rightarrow \pi N$  results calculated from using the models H and L are compared in Fig. 23. The photon-asymmetry ratios [Figs. 23(a) and 23(c)] are equally well described by both models. They yield, however, significant differences in describing the differential cross sections. In Fig. 23(b), we see that model H gives a much better description of the  $\pi^0$  differential cross sections in the high-energy region, but it slightly overestimates the cross sections at low energies. The  $\pi^+$  differential cross sections are better described by model H, as seen in Fig. 23(d). But the difficulty in reproducing the magnitude is not removed entirely.

The results in Fig. 23 suggest that our predictions do depend to some extent on the accuracy of the constructed  $\pi N$  model in describing the  $\pi N$  phase shifts. A natural next step is to extend the present model to include the inelastic chan-

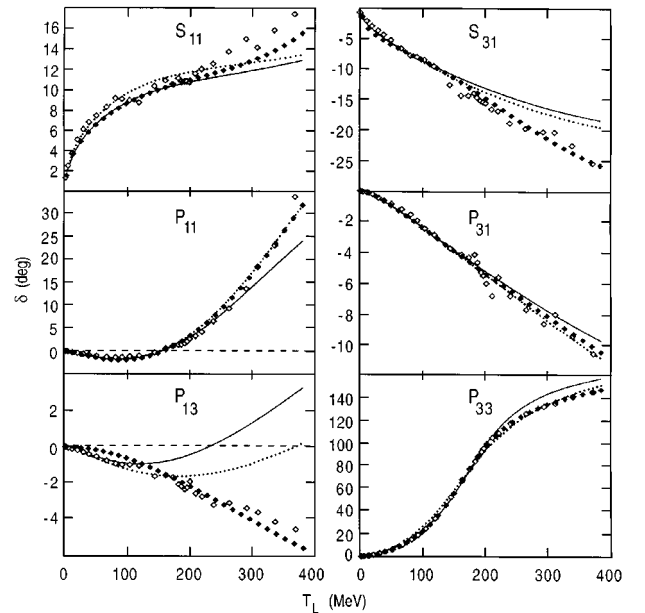


FIG. 22. The  $\pi N$  phase shifts calculated from model L (solid curves) and model H (dotted curves) are compared. The data are from Refs. [38] (solid squares) and [39] (open squares).  $T_L$  is pion energy in the laboratory frame.

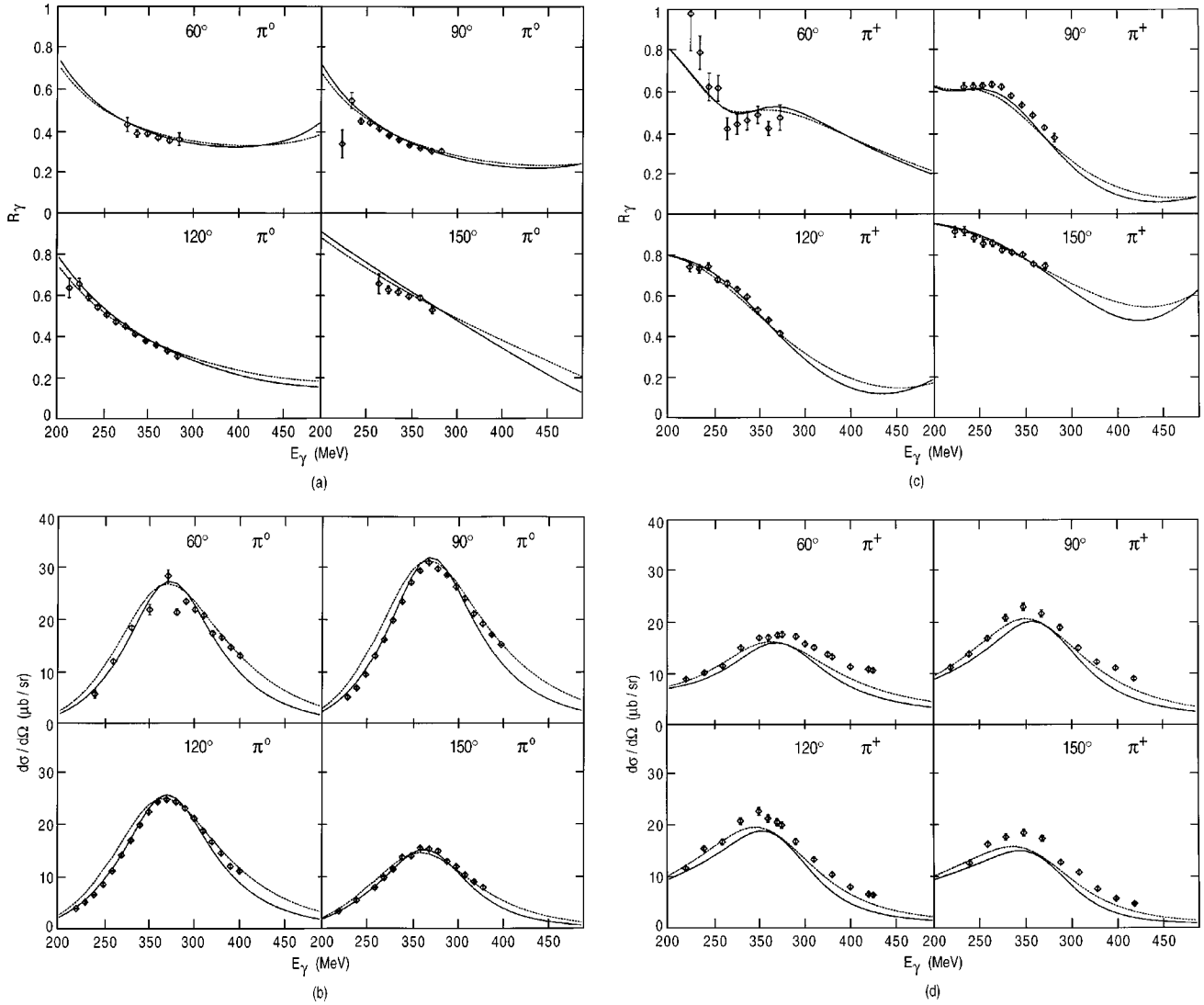


FIG. 23. Photon-asymmetry ratios and the differential cross sections for the  $\gamma p \rightarrow \pi^0 p$  (a) and (b) and  $\gamma p \rightarrow \pi^+ n$  (c) and (d) reactions. The solid (dotted) curves are from calculations using  $\pi N$  model L (model H). The parameters are  $(g_{\omega NN}, G_M, G_E) = (10.5, 1.85, +0.025)$ . The data are from Refs. [41,42].  $E_\gamma$  is the photon energy in the laboratory frame.

nels to obtain an accurate fit up to 400 MeV. This extension then will introduce inelastic pion photoproduction mechanisms, such as the  $\gamma N \rightarrow \pi \Delta \rightarrow \pi N$  process, which may be needed to resolve the difficulty in getting an accurate description of both the  $\pi^0$  and  $\pi^+$  processes. Such a coupled-channels approach must also include the effect due to the excitations of higher mass  $N^*$  nucleon resonances. This must be pursued in order to make progress in using the forthcoming data from CEBAF to test hadron models.

## VI. CONCLUSIONS AND FUTURE STUDIES

We have applied the unitary transformation method first proposed in Ref. [22] to derive from a model Lagrangian with  $N, \Delta, \pi, \rho, \omega,$  and  $\gamma$  fields an effective Hamiltonian consisting of bare  $\Delta \leftrightarrow \pi N$ ,  $\gamma N$  vertices and an energy-independent meson-exchange  $\pi N$  potential (Fig. 3) and  $\gamma N \rightarrow \pi N$  transition operator (Fig. 5). With the parameters listed in Table I for the strong form factors and the bare mass

of the  $\Delta$ , the model can give a good description of  $\pi N$  scattering phase shifts up to the  $\Delta$  excitation energy region. The only adjustable parameters in the resulting pion photoproduction amplitude are the coupling strengths  $G_E$  of the electric  $E2$  and  $G_M$  of the magnetic  $M1$  transitions of the bare  $\Delta \leftrightarrow \gamma N$  vertex and the less well-determined coupling constant  $g_{\omega NN}$  of the  $\omega$  meson. We have shown that the best reproduction of the recent LEGS data of the photon-asymmetry ratios of the  $\gamma p \rightarrow \pi^0 p$  reaction depends sensitively on these three parameters and yields  $G_M = 1.9 \pm 0.05$  and  $G_E = 0.0 \pm 0.025$  within the range  $7 \leq g_{\omega NN} \leq 10.5$ . Within these ranges of parameters, the predicted differential cross sections and photon-asymmetry ratios are in an overall good agreement with the data of  $\gamma p \rightarrow \pi^0 p$ ,  $\gamma p \rightarrow \pi^+ p$ , and  $\gamma n \rightarrow \pi^- p$  reactions from 180 MeV to the  $\Delta$  excitation region. The model, however, underestimates the  $\gamma N \rightarrow \pi N$  cross section at energies above the  $\Delta$  region. This is expected since the constructed model does not include inelastic channels, such as  $\pi \Delta$ ,  $\rho N$  channels, which should start to play a

significant role at energies above about 350 MeV. Including these channels could also be needed to resolve the difficulty in fitting  $P_{13}$   $\pi N$  phase shifts (Fig. 22). The constructed effective Hamiltonian is free of the nucleon renormalization problem and hence is suitable for nuclear many-body calculations.

We have also analyzed the  $K$ -matrix method which is commonly used to extract empirically the  $\gamma N \rightarrow \Delta$  transition amplitudes from the  $\gamma N \rightarrow \pi N$  data. It is found that the assumptions made in the  $K$ -matrix method [6] are consistent with our meson-exchange dynamical model. Our average value of the  $E2/M1$  ratio  $R_{EM} = (-1.8 \pm 0.9)\%$  is close to  $(-1.07 \pm 0.7)\%$  of Ref. [6]. The helicity amplitudes calculated from our bare  $\gamma N \rightarrow \Delta$  vertex are in good agreement with the predictions of the constituent quark models (Table IV). The differences between these bare amplitudes and the empirical values extracted from the data by using the  $K$ -matrix method are shown to be due to the nonresonant meson-exchange mechanisms. This suggests that the bare vertex interactions in our effective Hamiltonian can be identified with hadron models in which the  $\pi N$  and  $\pi\pi N$  ‘‘reaction’’ channels (both  $\pi$  and  $N$  are on their mass shell) are excluded in the calculation of the  $N^*$  excitation. Unfortunately we are not able to pin down the  $E2/M1$  ratio of the bare  $\gamma \rightarrow \Delta$  vertex by considering the existing data of photon-asymmetry ratios and differential cross sections. More precise data of other spin observables are needed to make progress. This will be pursued when the data becomes available, along with the extension of our approach to investigate pion electroproduction.

The unitary transformation method developed here can be extended to higher-energy regions for investigating higher mass  $N^*$  resonances. To proceed, we need to perform the unitary transformation up to second order in the coupling constants to account for the  $2\pi$  production channels. The resulting scattering equations will be defined in a larger coupled channel space  $N^* \oplus \pi N \oplus \gamma N \oplus \pi\pi N$ . This research program can be carried out in practice since the numerical methods for solving such a Faddeev-type coupled-channels equations (because of the presence of the three-body  $\pi\pi N$  unitary cut) have been well developed [53]. Our effort in this direction will be published elsewhere.

#### ACKNOWLEDGMENTS

We would like to thank Andy Sandorfi for his very stimulating discussions and providing experimental data. One of

the authors (T. S.) would like to thank the Theory Group of Physics Division at Argonne National Laboratory for the hospitality and discussions. This work is supported by the U.S. Department of Energy, Nuclear Physics Division, under Contract No. W-31-109-ENG-38, and by Grant-in-Aid of Scientific Research, the Ministry of Education, Science and Culture, Japan under Contract No. 07640405.

#### APPENDIX: DERIVATION OF $\pi N$ POTENTIAL

To see how the Feynman-amplitude-like expressions of Eqs. (3.12)–(3.16) are obtained in our approach, we give a detailed derivation of  $\pi N$  potential from the familiar Lagrangian

$$\mathcal{L} = \left[ -\frac{f_{\pi NN}}{m_\pi} \bar{\psi}(x) \gamma_5 \gamma^\mu \vec{\tau} \psi(x) \cdot \partial_\mu \vec{\phi}(x) + \frac{f_{\pi N \Delta}}{m_\pi} \bar{\psi}_\Delta^\mu(x) \vec{T} \psi(x) \cdot \partial_\mu \vec{\phi}(x) \right] + [\text{H.c.}], \quad (\text{A1})$$

where  $\psi(x)$ ,  $\psi_\Delta^\mu(x)$ , and  $\phi(x)$  are, respectively, the field operators for  $N$ ,  $\Delta$ , and  $\pi$ ,  $\vec{T}$  is the  $\Delta \rightarrow N$  isospin transition operator, and [H.c.] means taking the Hermitian conjugate of the first term. By applying the canonical quantization procedure (see Sec. III about the problem concerning the  $\Delta$  field), we can derive a Hamiltonian from Eq. (A1). The resulting Hamiltonian can be written as

$$H = H_0 + H_I, \quad (\text{A2})$$

with

$$H_I = H_I^P + H_I^Q, \quad (\text{A3})$$

where  $H^P(H^Q)$  describes processes which can (cannot) take place in free space. Explicitly, we can write in second quantization form

$$H_I^P = \sum_\alpha \int \frac{1}{(2\pi)^{3/2}} \frac{1}{\sqrt{2E_\pi(k)}} d\vec{p} d\vec{p}' d\vec{k} \left\{ i \frac{f_{\pi N \Delta}}{m_\pi} \sqrt{\frac{m_N}{E_N(p)}} \sqrt{\frac{m_\Delta}{E_\Delta(p')}} \bar{\omega}_p^{\mu'} T_\alpha u_{\vec{p}} k_\mu \Delta_{\vec{p}'}^\dagger b_{\vec{p}} a_{\vec{k}\alpha} \delta(\vec{p} + \vec{k} - \vec{p}') \right. \\ \left. - i \frac{f_{\pi N \Delta}}{m_\pi} \sqrt{\frac{m_N}{E_N(p')}} \sqrt{\frac{m_\Delta}{E_\Delta(p)}} \bar{u}_{\vec{p}'} T_\alpha^\dagger \omega_p^\mu k_\mu b_{\vec{p}}^\dagger \Delta_{\vec{p}} a_{\vec{k}\alpha}^\dagger \delta(\vec{p} - \vec{k} - \vec{p}') \right\}, \quad (\text{A4})$$

where  $a_{\vec{k}\alpha}^\dagger$ ,  $b_{\vec{p}}^\dagger$ , and  $\Delta_{\vec{p}}^\dagger$  are, respectively, the creation operators for  $\pi$ ,  $N$ , and  $\Delta$  states,  $\alpha$  is the pion isospin index, and  $u$  and  $\omega^\mu$  are, respectively, the spinors of Dirac and Rarita-Schwinger fields. Clearly,  $H^P$  describes the  $\Delta \leftrightarrow \pi N$  real processes [similar to Figs. 1(a) and 1(b) with the change  $\sigma \rightarrow \Delta$ ] which can take place in free space. On the other hand, the virtual processes [similar to Figs. 1(c)–1(f)] are due to the Hamiltonian

$$\begin{aligned}
H_I^Q = & \sum_{\alpha} \int \frac{1}{(2\pi)^{3/2}} \frac{1}{\sqrt{2E_{\pi}(k)}} d\vec{p} d\vec{p}' d\vec{k} \\
& \times \left[ i \frac{f_{\pi NN}}{m_{\pi}} \sqrt{\frac{m}{E_N(p)}} \sqrt{\frac{m}{E_N(p')}} \{ \bar{u}_{\vec{p}'} \gamma_5 \tau^{\alpha} \mathbf{k} u_{\vec{p}} b_{\vec{p}}^{\dagger}, b_{\vec{p}} [ -\delta(\vec{p}' - \vec{p} - \vec{k}) a_{\vec{k}, \alpha} + \delta(\vec{p}' - \vec{p} + \vec{k}) a_{\vec{k}, \alpha}^{\dagger} ] \right. \\
& + \bar{u}_{\vec{p}} \gamma_5 \tau^{\alpha} \mathbf{k} v_{\vec{p}} b_{\vec{p}}^{\dagger}, d_{\vec{p}}^{\dagger} [ -\delta(\vec{p}' + \vec{p} - \vec{k}) a_{\vec{k}, \alpha} + \delta(\vec{p}' + \vec{p} + \vec{k}) a_{\vec{k}, \alpha}^{\dagger} ] + \bar{v}_{\vec{p}'} \gamma_5 \mathbf{k} \tau^{\alpha} u_{\vec{p}} d_{\vec{p}}^{\dagger}, b_{\vec{p}} \\
& \times [ -\delta(-\vec{p}' - \vec{p} - \vec{k}) a_{\vec{k}, \alpha} + \delta(-\vec{p}' - \vec{p} + \vec{k}) a_{\vec{k}, \alpha}^{\dagger} ] + \bar{v}_{\vec{p}'} \gamma_5 \mathbf{k} \tau^{\alpha} v_{\vec{p}} d_{\vec{p}}^{\dagger}, d_{\vec{p}}^{\dagger} [ -\delta(-\vec{p}' + \vec{p} - \vec{k}) a_{\vec{k}, \alpha} + \delta(-\vec{p}' + \vec{p} + \vec{k}) a_{\vec{k}, \alpha}^{\dagger} ] \} \\
& - i \frac{f_{\pi N \Delta}}{m_{\pi}} \sqrt{\frac{m}{E_N(p')}} \sqrt{\frac{m_{\Delta}}{E_{\Delta}(p')}} \{ \bar{\omega}_{\vec{p}'}^{\mu} u_{\vec{p}} k_{\mu} \Delta_{\vec{p}}^{\dagger}, b_{\vec{p}} \delta(\vec{p}' - \vec{p} + \vec{k}) a_{\vec{k}, \alpha}^{\dagger} + \bar{\omega}_{\vec{p}'}^{\mu} \cdot v_{\vec{p}} k_{\mu} \Delta_{\vec{p}}^{\dagger}, d_{\vec{p}}^{\dagger} \delta(\vec{p}' + \vec{p} + \vec{k}) a_{\vec{k}, \alpha}^{\dagger} \} \\
& + i \frac{f_{\pi N \Delta}}{m_{\pi}} \sqrt{\frac{m}{E_N(p')}} \sqrt{\frac{m_{\Delta}}{E_{\Delta}(p')}} \{ \bar{u}_{\vec{p}} \omega_{\vec{p}}^{\mu} k_{\mu} b_{\vec{p}}^{\dagger}, \Delta_{\vec{p}} \delta(\vec{p}' - \vec{p} - \vec{k}) a_{\vec{k}, \alpha} + \bar{v}_{\vec{p}'} \omega_{\vec{p}}^{\mu} k_{\mu} d_{\vec{p}}^{\dagger}, \Delta_{\vec{p}} \delta(-\vec{p}' - \vec{p} - \vec{k}) a_{\vec{k}, \alpha} \} \right]. \quad (\text{A5})
\end{aligned}$$

Note that the above equation includes an antinucleon spinor  $v$ , which is included to maintain the relativistic feature of the starting quantum field theory.

To proceed, we need to derive the unitary transformation operator  $S$ . By the procedures outlined in Sec. II,  $S$  is related to  $H_I^Q$ . Hence, the actual task of deriving the  $\pi N$  potential is to evaluate Eq. (2.23) from the  $H_I^P$  and  $H_I^Q$  defined above. Let us first focus on the first four  $\pi NN$  coupling terms of Eq. (A5). We need to consider

$$|i\rangle = b_{\vec{p}}^{\dagger} a_{\vec{k}\alpha}^{\dagger} |0\rangle,$$

$$|f\rangle = b_{\vec{p}}^{\dagger} a_{\vec{k}\alpha}^{\dagger} |0\rangle.$$

The allowed intermediate states in Eq. (2.23) are  $|n\rangle = b_{\vec{p}_n}^{\dagger} |0\rangle$ ,  $b_{\vec{p}_m}^{\dagger} a_{\vec{k}'\alpha}^{\dagger} a_{\vec{k}\alpha}^{\dagger} |0\rangle$  for the first term, and  $|n\rangle = d_{-\vec{p}_n}^{\dagger} b_{\vec{p}}^{\dagger}, b_{\vec{p}}^{\dagger} a_{\vec{k}\alpha}^{\dagger} a_{\vec{k}'\alpha}^{\dagger} |0\rangle$ ,  $d_{-\vec{p}_m}^{\dagger} b_{\vec{p}}^{\dagger}, b_{\vec{p}}^{\dagger} |0\rangle$  for the other three terms involving the antinucleon component  $v$ . Substituting these intermediate states into Eq. (2.23) and performing straightforward operator algebra, we then obtain

$$\langle \vec{k}' \alpha', \vec{p}' | H_I^P | \vec{k} \alpha, \vec{p} \rangle = \frac{(f_{\pi NN}/m_{\pi})^2}{(2\pi)^3} \frac{1}{\sqrt{2E_{\pi}(k')}} \sqrt{\frac{m_N}{E_N(p')}} \bar{u}_{\vec{p}'} \left[ \sum_{i=1}^4 M^{(i)} \right] \sqrt{\frac{m_N}{E_N(p)}} \frac{1}{\sqrt{2E_{\pi}(k)}} u_{\vec{p}}, \quad (\text{A6})$$

where

$$M^{(1)} = \frac{m_N}{E_N(p_n)} \gamma_5 \mathbf{k}' \tau_{\alpha} u_{\vec{p}_n} \bar{u}_{\vec{p}_n} \gamma_5 \mathbf{k} \tau_{\alpha} \frac{1}{2} \left[ \frac{1}{E_N(p) - E_N(p_n) + E_{\pi}(k)} - \frac{1}{E_N(p_n) - E_N(p') - E_{\pi}(k')} \right],$$

with  $\vec{p}_n = \vec{k} + \vec{p} = \vec{k}' + \vec{p}'$ ,

$$M^{(2)} = \frac{m_N}{E_N(p_m)} \gamma_5 \mathbf{k} \tau_{\alpha} u_{\vec{p}_m} \bar{u}_{\vec{p}_m} \gamma_5 \mathbf{k}' \tau_{\alpha'} \frac{1}{2} \left[ \frac{1}{E_N(p) - E_N(p_m) - E_{\pi}(k')} - \frac{1}{E_N(p_m) - E_N(p') + E_N(k)} \right],$$

with  $\vec{p}_m = \vec{p} - \vec{k}' = \vec{p}' - \vec{k}$ , and

$$M^{(3)} = -\frac{m_N}{E_N(p_n)} \gamma_5 \mathbf{k}' \tau_{\alpha} v_{-\vec{p}_n} \bar{v}_{-\vec{p}_n} \gamma_5 \mathbf{k} \tau_{\alpha} \frac{1}{2} \left[ \frac{1}{-E_N(p') - E_N(p_n) - E_{\pi}(k')} - \frac{1}{E_N(p) + E_N(p_n) + E_{\pi}(k)} \right],$$

$$M^{(4)} = -\frac{m_N}{E_N(p_m)} \gamma_5 \mathbf{k} \tau_{\alpha} v_{-\vec{p}_m} \bar{v}_{-\vec{p}_m} \gamma_5 \mathbf{k}' \tau_{\alpha'} \frac{1}{2} \left[ \frac{1}{-E_N(p') - E_N(p_m) + E_{\pi}(k)} - \frac{1}{E_N(p) + E_N(p_m) - E_{\pi}(k')} \right].$$

By using the properties that

$$\frac{m_N}{E_N(p)} u_{\vec{p}} \bar{u}_{\vec{p}} = \frac{1}{2E_N(p)} [m_N + \gamma_0 E_N(p) - \vec{\gamma} \cdot \vec{p}],$$

$$\frac{m_N}{E_N(p)} v_{\vec{p}} \bar{v}_{\vec{p}} = \frac{1}{2E_N(p)} [-m_N + \gamma_0 E_N(p) - \vec{\gamma} \cdot \vec{p}],$$

(A7)

one can easily show that, for an arbitrary  $p_0$ ,

$$\begin{aligned} \frac{m_N}{E_N(p_n)} u_{\vec{p}_n} \bar{u}_{\vec{p}_n} \frac{1}{p_0 - E_N(p_n)} + \frac{m_N}{E_N(p_n)} v_{-\vec{p}_n} \bar{v}_{-\vec{p}_n} \frac{1}{p_0 + E_N(p_n)} &= \frac{1}{2E_N(p_n)} \left[ (m_N - \vec{\gamma} \cdot \vec{p}_n) \left( \frac{1}{p_0 - E_N(p_n)} - \frac{1}{p_0 + E_N(p_n)} \right) \right. \\ &\quad \left. + \gamma_0 E_N(p_n) \left( \frac{1}{p_0 - E_N(p_n)} + \frac{1}{p_0 + E_N(p_n)} \right) \right] \\ &= \frac{1}{p_0^2 - E_N^2(p_n)} [m_N - \vec{\gamma} \cdot \vec{p}_n + \gamma_0 p_0] = \frac{\not{p}_n + m_N}{p_n^2 - m_N^2} = \frac{1}{\not{p}_n - m_N}, \end{aligned} \quad (\text{A8})$$

where  $p_n = (p_0, \vec{p}_n)$ .

By using Eq. (A8), we can combine various propagators in Eq. (A6) to obtain

$$\sum_{i=1}^4 M^{(i)} = \gamma_5 \not{k}' \tau_{\alpha'} \frac{1}{2} \left[ \frac{1}{(\not{p} + \not{k}) - m_N} + \frac{1}{(\not{p} + \not{k}') - m_N} \right] \gamma_5 \not{k} \tau_{\alpha} + \gamma_5 \not{k} \tau_{\alpha} \frac{1}{2} \left[ \frac{1}{(\not{p} - \not{k}') - m_N} + \frac{1}{(\not{p}' - \not{k}) - m_N} \right] \gamma_5 \not{k}' \tau_{\alpha'},$$

where  $p = (E_N(p), \vec{p})$  and  $k = (E_{\pi}(k), \vec{k})$ . The above result looks remarkably simple. It resembles very much the usual Feynman amplitudes, except that the intermediate nucleon propagator is the average of two Dirac propagators for the momenta evaluated using the incoming or outgoing  $\pi N$  momentum variables.

The evaluation of the  $\Delta$  terms is much more involved, but yields a similar form as given in Eqs. (3.15) and (3.16). Similar derivations can also be carried out to define the  $\pi N$  interactions, Eq. (3.14), due to the  $\rho$  meson.

- 
- [1] See review by A. Donnachie, in *High Energy Physics*, edited by E. Burhop (Academic Press, New York, 1972), Vol. 5, p. 1.
- [2] See review by T.-S. H. Lee, in *Baryon '92*, edited by Moshe Gai (World Scientific, Singapore, 1993), p. 99.
- [3] Herman Feshbach, *Theoretical Nuclear Physics, Nuclear Reactions* (Wiley, New York, 1992).
- [4] M. G. Olsson and E. T. Osypowski, Nucl. Phys. **B87**, 399 (1975); Phys. Rev. D **17**, 174 (1978).
- [5] R. M. Davidson, N. C. Mukhopadhyay, and R. S. Wittman, Phys. Rev. D **43**, 71 (1991).
- [6] R. M. Davidson and N. C. Mukhopadhyay, Phys. Rev. D **42**, 20 (1990).
- [7] Z. Li, R. A. Arndt, L. D. Roper, and R. L. Workman, Phys. Rev. C **47**, 2759 (1993).
- [8] R. Machleidt, in *Advances in Nuclear Physics*, edited by J.W. Negele and E. Vogt (Plenum, New York, 1989), Chap. 2, Vol. 19.
- [9] D. O. Riska and G. E. Brown, Phys. Lett. **32B**, 193 (1970).
- [10] M. Chemtob and M. Rho, Nucl. Phys. **A163**, 1 (1971).
- [11] D. Lohse, J. W. Durso, K. Holinde, and J. Speth, Nucl. Phys. **A516**, 513 (1990).
- [12] B. C. Pearce and B. Jennings, Nucl. Phys. **A528**, 655 (1991).
- [13] C. T. Hung, S. N. Yang, and T.-S. H. Lee, J. Phys. G **20**, 1531 (1994).
- [14] C. Schütz, J. W. Durso, K. Holinde, and J. Speth, Phys. Rev. C **49**, 2671 (1994).
- [15] H. Tanabe and K. Ohta, Phys. Rev. C **31**, 1876 (1985).
- [16] S. N. Yang, J. Phys. G **11**, L205 (1985).
- [17] S. Nozawa, B. Blankleider, and T.-S. H. Lee, Nucl. Phys. **A513**, 459 (1990).
- [18] T.-S. H. Lee and B. C. Pearce, Nucl. Phys. **A530**, 532 (1991).
- [19] F. Gross and Y. Surya, Phys. Rev. C **47**, 703 (1993).
- [20] Y. Surya and F. Gross, Phys. Rev. C **53**, 2422 (1996).
- [21] M. Araki and I. R. Afnan, Phys. Rev. **36**, 250 (1987); C. van Antwerpen and I. Afnan, *ibid.* C **52**, 554 (1995).
- [22] T. Sato, M. Doi, N. Odagawa, and H. Ohtsubo, Few-Body Syst. Suppl. **5**, 254 (1992); T. Sato, M. Kobayashi, and H. Ohtsubo (unpublished).
- [23] T.-S. H. Lee and A. Matsuyama, Phys. Rev. C **32**, 516 (1986); **36**, 1459 (1987).
- [24] As reviewed by A. Klein and T.-S. H. Lee, Phys. Rev. D **10**, 4308 (1974).
- [25] I. Tamm, J. Phys. (Moscow) **9**, 449 (1945); S. M. Dancoff, Phys. Rev. **78**, 382 (1950).
- [26] N. Fukuda, K. Sawada, and M. Taketani, Prog. Theor. Phys. **12**, 156 (1954).
- [27] S. Okubo, Prog. Theor. Phys. **12**, 603 (1953).
- [28] K. Ohta and M. Wakamatsu, Prog. Theor. Phys. **55**, 131 (1976).
- [29] M. Gari and H. Hyuga, Z. Phys. A **277**, 291 (1976).
- [30] T. Sato, M. Kobayashi, and H. Ohtsubo, Prog. Theor. Phys. **68**, 840 (1982).
- [31] W. Glöckle and L. Müller, Phys. Rev. C **23**, 1183 (1981).
- [32] L. Müller, Nucl. Phys. **A360**, 331 (1981).
- [33] T. Sato, K. Tamura, T. Niwa, and H. Ohtsubo, J. Phys. G **17**, 303 (1991).
- [34] K. Tamura, T. Niwa, T. Sato, and H. Ohtsubo, Nucl. Phys. **A536**, 597 (1992).
- [35] H. Gacilazo and T. Mizutani,  *$\pi NN$  System* (World Scientific, Singapore, 1990).
- [36] V. Bernard, N. Kaiser, and U. Meissner, Nucl. Phys. **B383**, 442 (1992); V. Bernard, N. Kaiser, T.-S. H. Lee, and U. Meissner, Phys. Rev. Lett. **70**, 387 (1993); Phys. Rep. **246**, 315 (1994).
- [37] S. Weinberg, Physica A **96**, 327 (1979).
- [38] R. A. Arndt, J. M. Ford, and L. D. Roper, Phys. Rev. D **32**, 1085 (1985).



- [39] G. Höhler, F. Kaiser, R. Koch, and E. Pietarinen, *Handbook of Pion-Nucleon Scattering*, Physics Data Vol. 12-1 (Karlsruhe, 1979).
- [40] R. Koch and E. Pietarinen, Nucl. Phys. **A336**, 331 (1980).
- [41] LEGS Collaboration, A. M. Sandorfi *et al.*, Few Body Syst. Suppl. **7**, 317 (1994); LEGS Data Release No. L7a8.0, (1994); A.M. Sandorfi (private communication).
- [42] H. Genzel *et al.*, Z. Phys. A **268**, 43 (1974).
- [43] D. Menze, W. Pfeil, and R. Wilcke, ZAED Compilation of Pion Photoproduction Data, University of Bonn, 1977.
- [44] P. Dougan *et al.*, Z. Phys. A **276**, 155 (1976).
- [45] Review of particle properties, L. Montanet *et al.*, Phys. Rev. D **50**, 1173 (1994), p. 1710.
- [46] N. Isgur and G. Karl, Phys. Rev. D **19**, 2653 (1979); R. Konik and N. Isgur, *ibid.* **21**, 1868 (1990).
- [47] S. Capstick, Phys. Rev. D **46**, 2864 (1992).
- [48] R. Bijker, F. Iachello, and A. Leviatan, Ann. Phys. (N.Y.) **236**, 69 (1994).
- [49] F. E. Close and Z. Li, Phys. Rev. D **42**, 2194 (1990).
- [50] S. Capstick and B. D. Keister, Phys. Rev. D **51**, 3598 (1995).
- [51] O. Hanstein, D. Drechsel, and L. Tiator, Mainz report, 1996.
- [52] J. D. Bjorken and S. D. Drell, *Relativistic Quantum Mechanics* (McGraw-Hill, New York, 1964).
- [53] As reviewed by R. D. Amado and R. Aaron, in *Modern Three-Hadron Physics*, edited by A. W. Thomas, Topics in Current Physics (Springer-Verlag, Berlin, 1977).
- [54] We use Edmond's convention  $\langle J' M' | T_{kq} | J M \rangle = (-1)^{2k} \langle J' M' | J k M q \rangle / \sqrt{2J'+1} \langle J' || T_k || J \rangle$ .
- [55] David Lurié, *Particles and Fields* (Wiley, New York, 1968).
- [56] M. Benmerrouche, R. M. Davidson, and N. C. Mukhopadhyay, Phys. Rev. C **39**, 2339 (1989).
- [57] F. A. Berends and A. Donnachie, Nucl. Phys. **B84**, 342 (1975).